

## Response to reviews

Comments to the Author:

The authors have reasonably addressed the comments of the referees. However, a number of minor alterations are needed before the manuscript and its Supplement can be published in ACP.

**We thank the editor for all the corrections. Changes are made accordingly.**

For the main text:

Page 0, line 3: The affiliation is missing for Pauliquevis.

Line 36: Replace “BVOC” by “BVOCs”.

Line 86: Replace “located 60 km NNW of Manaus and faced” by “is located 60 km NNW of Manaus and faces”.

Line 112: Replace “because their” by “because of their”.

Line 113: Replace “(PMF; (Paatero and Tapper, 1994))” by “(PMF) (Paatero and Tapper, 1994)”.

Line 143: Replace “larger (up” by “larger levels (up”.

Line 172: Replace “from Atlantic” by “from the Atlantic”.

Line 178: Replace “Supplement. Other” by “Supplement). Other”.

Line 182: Replace “on average,” by “, on average,”.

Line 269: Replace “on order” by “on the order”.

Line 270: Replace “highly-oxidizedorganic” by “highly-oxidized organic”.

Line 271: Replace “AMAZE-08(Chen” by “AMAZE-08 (Chen”.

Line 280: Replace “correlation value” by “correlation values”.

**Changes are made to address the above comments.**

Line 299: It is unclear what is meant by “statistical factories”. Should it perhaps be “statistical factors” instead?

**Yes, it should be “factors” instead of “factories”. This change is made.**

Page 18, lines 7-4 from bottom: “Andreae (2007)” should come before “Andreae et al. (1990)”.

**This change is made.**

Pages 19-23: “Poschl” should be replaced by “Pöschl” (on 6 occasions).

**We have replaced “Poschl” by “Pöschl” in the main text as well as in the Supplement.**

For the Supplementary Material:

Page 1, line 7 from bottom: Replace “excluded from” by “and excluded from”.

Page 2, line 11: Replace “readily undergo” by “readily undergoes”.

Page 2, line 12: Replace “lead much” by “lead to much”.

Page 2, line 2 from bottom: Replace “IC, and PIXE” by “ion chromatography (IC), and particle-induced X-ray emission (PIXE)”.

Page 3, line 15: Replace “Roldin” by “Roldin et al.”.

Page 4, line 4: Replace “from SFU” by “from the SFU”.

Page 4, line 5: Replace “ion chromatography (IC) for” by “IC for”.

Page 4, line 7: Replace “particle-induced X-ray emission (PIXE) for” by “PIXE for”.

Page 5, last line: Replace “0.006 I” by “0.006 i”.

Page 6, line 8: Replace “driven force” by “driving force”.

Page 7, line 2: Replace “having signal-to-noise” by “having a signal-to-noise”.

Page 8, line 2: Replace “strongly correlation” by “strong correlation”.

**Changes are made to address the above comments.**

Pages 11-12: There is no reference made within the text to the following references that are in the Reference list: “Docherty et al. (2008)”, “Gomez-Gonzalez et al. (2008)”, “Iinuma et al. (2009)”, and “Surratt et al. (2008)”.

Those uncited references are removed.

Page 14, line 4: Replace “mass distributions” by “mass size distributions”.

Page 15, line 8 from bottom: Replace “chloride respectively and” by “chloride, respectively, and”.

Changes are made to address the above comments.

# Submicron Particle Mass Concentrations and Sources in the Amazonian Wet Season (AMAZE-08)

Q. Chen<sup>1,\*</sup>, D. K. Farmer<sup>2,\*\*</sup>, L. V. Rizzo<sup>3,\*\*\*</sup>, T. Pauliquevis<sup>3,\*\*\*</sup>, M. Kuwata<sup>1,\*\*\*\*</sup>, T. G. Karl<sup>34,\*\*\*\*\*</sup>, A. Guenther<sup>34,\*\*\*\*\*</sup>, J. D. Allan<sup>45</sup>, H. Coe<sup>45</sup>, M. O. Andreae<sup>56</sup>, U. Pöschl<sup>56</sup>, J. L. Jimenez<sup>2</sup>, P. Artaxo<sup>67</sup>, S. T. Martin<sup>1</sup>

(1) School of Engineering and Applied Sciences & Department of Earth and Planetary Sciences, Harvard University, Cambridge, MA, USA

(2) Department of Chemistry and Biochemistry & Cooperative Institute for Research in Environmental Science, University of Colorado, Boulder, CO, USA

(3) Department of Exact and Earth Sciences, Federal University of São Paulo, Diadema, Brazil

~~(43)~~ National Center for Atmospheric Research, Boulder, CO, USA

~~(54)~~ National Centre for Atmospheric Science & School of Earth, Atmospheric and Environmental Sciences, University of Manchester, Manchester, UK

~~(65)~~ Max Planck Institute for Chemistry, Mainz, Germany

~~(76)~~ Applied Physics Department & Atmospheric Science Department, University of São Paulo, São Paulo, Brazil

\*Now at State Key Joint Laboratory of Environmental Simulation and Pollution Control, College of Environmental Sciences and Engineering, Peking University, Beijing, 100871, China

\*\*Now at Department of Chemistry, Colorado State University, Fort Collins, CO, USA

~~\*\*\*Now at Department of Exact and Earth Sciences, Federal University of São Paulo, Diadema, Brazil~~

\*\*\*\*Now at Nanyang Technological University and Earth Observatory of Singapore, Singapore

\*\*\*\*\*Now at Institute of Meteorology and Geophysics, University of Innsbruck, Austria

\*\*\*\*\*Now at Atmospheric Sciences and Global Change Division, Pacific Northwest National Laboratory, Richland, WA, USA.

Manuscript submitted to *Atmospheric Chemistry and Physics*

Correspondence to: S.T. Martin (scot\_martin@harvard.edu) and P. Artaxo (artaxo@if.usp.br)

1 **Abstract**

2           Real-time mass spectra of the non-refractory species in submicron aerosol particles were  
3 recorded in a tropical rainforest in the central Amazon basin during the wet season from  
4 February to March 2008, as a part of the Amazonian Aerosol Characterization Experiment  
5 (AMAZE-08). Organic material accounted on average for more than 80% of the non-refractory  
6 submicron particle mass concentrations during the period of measurements. There was  
7 insufficient ammonium to neutralize sulfate. In this acidic, isoprene-rich, HO<sub>2</sub>-dominant  
8 environment positive-matrix factorization of the time series of particle mass spectra identified  
9 four statistical factors to account for the 99% variance of the signal intensities of the organic  
10 constituents. The first factor was identified as associated with regional and local pollution and  
11 labeled as “HOA” for its hydrocarbon-like characteristics. A second factor was associated with  
12 long-range transport and labeled as “OOA-1” for its oxygenated characteristics. A third factor,  
13 labeled “OOA-2,” was implicated as associated with the reactive uptake of isoprene oxidation  
14 products, especially of epoxydiols to acidic haze, fog or cloud droplets. A fourth factor, labeled  
15 as “OOA-3,” was consistent with an association to the fresh production of secondary organic  
16 material (SOM) by a mechanism of gas-phase oxidation of biogenic volatile organic precursors  
17 followed by gas-to-particle conversion of the oxidation products. The suffixes 1, 2, and 3 on the  
18 OOA labels signify ordinal ranking with respect to the extent of oxidation represented by the  
19 factor. The process of aqueous-phase oxidation of water-soluble products of gas-phase  
20 photochemistry might also have been associated to some extent with the OOA-2 factor. The  
21 campaign-average factor loadings were in a ratio of 1.4:1 for OOA-2:OOA-3, suggesting the  
22 comparable importance of particle-phase compared to gas-phase pathways for the production of  
23 SOM during the study period.

## 47 | **11. Introduction**

48           Aerosol particles in the atmosphere make an important contribution to the Earth's  
49 radiation budget (IPCC, 2013). They can directly scatter and absorb shortwave and longwave  
50 radiation, and they can indirectly affect radiative forcing and precipitation by modifying cloud  
51 properties. The assessment of the impact of human perturbations on climate requires an  
52 understanding of the natural functioning of the aerosol-cloud-climate system. During the wet  
53 season, the pristine Amazon basin provides a unique environment for studying the sources and  
54 atmospheric evolution of natural aerosol particles and hence understanding the role of aerosol  
55 particles in biosphere-atmosphere interactions (Andreae, 2007; Martin et al., 2010a).

56           Tropical forest emissions and long-range transport from outside of the basin are major  
57 contributors to the number and mass budgets of Amazonian aerosol particles during the wet  
58 season because regional biomass burning emission is largely suppressed by heavy rainfall  
59 (Martin et al., 2010a). The forest ecosystem emits biogenic volatile organic compounds  
60 (BVOCs) that can be oxidized in the atmosphere, principally by reaction with photochemically  
61 produced hydroxyl radical and ozone molecules. Some of the oxidized products have sufficiently  
62 low vapor pressures to condense and produce SOM in the particle phase. Moreover, in haze, fog,  
63 and cloud droplets, the production of organic acids and oligomers can occur from the OH-  
64 initiated aqueous-phase oxidation of the photooxidation products of isoprene, e.g., glyoxal,  
65 methacrolein (MACR), and methylvinyl ketone (MVK) (Lim et al., 2010), as well as from the  
66 acid-catalyzed reactive uptake of epoxydiol isomers (IEPOX) (Surratt et al., 2010; Lin et al.,  
67 2012). For SOM produced by these aqueous-phase pathways, a fraction of the mass can remain  
68 in the particle phase after dehumidification. In addition, the forest also directly emits primary  
69 biological particles containing potassium, phosphorus, sugars, sugar alcohols, and fatty acids,

70 including an upper limit of a 20% contribution to the submicron organic mass concentration  
71 (Graham et al., 2003a; Elbert et al., 2007; Schneider et al., 2011; Pöhlker et al., 2012). The forest  
72 also emits gases important to the particle mass concentrations of inorganic ions. For example,  
73 ammonia partitions from the gas phase to acidic particles (Trebs et al., 2005). Reduced sulfur  
74 gases undergo atmospheric oxidation to produce sulfuric acid that condenses to the particle  
75 phase (Andreae et al., 1990).

76         The Amazonian Aerosol Characterization Experiment 2008 (AMAZE-08) investigated  
77 the sources and properties of Amazonian particles (Martin et al., 2010b). Evidence from  
78 AMAZE-08 led to the conclusion that there is a large-scale contribution of biogenic SOM to the  
79 mass concentration of submicron aerosol particles during the wet season (Chen et al., 2009;  
80 Martin et al., 2010b; Pöschl et al., 2010; Schneider et al., 2011). In particular, Chen et al. (2009)  
81 demonstrated that on order of 90% of the organic material of submicron Amazonian particles  
82 arises from the in-Basin production of biogenic SOM. Primary biogenic particles enriched in  
83 potassium salts and emitted by fungal spores as 10 to 20 nm dried particles possibly provide  
84 surfaces for the condensation of SOM from the gas phase (Pöhlker et al., 2012). These bio-  
85 related particles participate in the regulation of the hydrological cycle of the forest by serving as  
86 nuclei for cloud formation and subsequent precipitation (Gunthe et al., 2009; Prenni et al., 2009).  
87 In addition to particle production tied to the forest ecosystem, lidar and satellite observations  
88 provide evidence of episodic long-range advection of African smoke and Saharan dust (Ben-Ami  
89 et al., 2010; Baars et al., 2011). These intrusions are temporally consistent with increases of  
90 heavily oxidized organic particles observed by Chen et al. (2009), indicative of long atmospheric  
91 residence times, as well as increases in the concentrations of ice nuclei observed by Prenni et al.  
92 (2009).

116 The present study analyzes multiple data sets collected during AMAZE-08 in relation to  
117 one another and in the context of the chemistry and properties of submicron particles in the  
118 Amazon basin during the wet season. A focus topic is the relative importance of aqueous-phase  
119 reactions compared to gas-phase oxidation followed by condensation to the production of SOM  
120 mass concentration. The relative importance of these two pathways remains poorly understood  
121 (Martin et al., 2010a; Ervens et al., 2011). On the one hand, condensational growth has been  
122 reported as an important pathway of the biogenic SOM production (Graham et al., 2003a). On  
123 the other hand, a significant role of liquid-phase processing for Amazonian aerosol particles is  
124 proposed (Pöhlker et al., 2012). In the current study, positive-matrix factorization of the time  
125 series of particle mass spectra is used to identify statistical factors that differ in mass spectral  
126 patterns (Zhang et al., 2011). The properties of these factors, in conjunction with the auxiliary  
127 data sets, are used to investigate the relative importance of different possible sources of  
128 submicron organic material in Amazonia during the wet season.

## 129 **22. Site and Instrument Description**

130 Ground-based measurements were carried out at a rainforest site during the wet season  
131 from 7 February to 13 March 2008 (Martin et al., 2010b). The site (02 °35.68 'S, 60 °12.56 'W,  
132 110 m above sea level) is located 60 km NNW of Manaus and ~~faeed~~ faces 1600 km of nearly  
133 pristine forest to the east to the Atlantic Ocean. The site was accessed by a 34-km unpaved road  
134 from Highway 174 (Fig. S1). The ten-day back trajectories indicated that during the  
135 measurement period the air masses mainly originated from the northeast over the Atlantic Ocean  
136 in the direction of Cape Verde and the Canary Islands. Air was sampled at the top of a tower  
137 ("TT34"; 38.75 m) above the forest canopy (33 m). Instrumentation deployed during AMAZE-  
138 08 is described in Martin et al. (2010b).

Formate  
or gramm

139           The present study focuses mostly on the statistical analysis of the data sets of an  
140 Aerodyne high-resolution Aerosol Mass Spectrometer (HR-AMS) in the context of  
141 complementary data sets of other instruments. Mass concentrations were adjusted to standard  
142 temperature and pressure (noted as STP; 273.15 K and  $10^5$  Pa), which were approximately 10%  
143 greater than those at calibration conditions (299.3 K and 100591.7 Pa). Details on sampling by  
144 the AMS and data analysis are provided in Chen et al. (2009) and Sect. A of the Supplement.  
145 The description of other concurrent measurements and the comparisons among the  
146 measurements are provided in Sect. B of the Supplement. Table S1 lists the regression  
147 coefficients for the multi-instrument data comparison. For a collection efficiency of unity, the  
148 AMS data agreed within measurement uncertainty with the other data sets, which is consistent  
149 with the understanding that liquid particles do not bounce from the AMS vaporizer (Matthew et  
150 al., 2008). Images of filter samples showed that spherical organic particles, appearing as like-  
151 liquid droplets, were the main population in the submicron fraction of the ambient particle  
152 population for AMAZE-08 (Pöschl et al., 2010).

153           Atomic ratios of oxygen-to-carbon (O:C), hydrogen-to-carbon (H:C), nitrogen-to-carbon  
154 (N:C), and sulfur-to-carbon (S:C), as well as the organic-mass-to-organic-carbon (OM:OC)  
155 ratios, were calculated from the high-resolution “W-mode” data (Aiken et al., 2008). The ratios  
156 were corrected by the method of Canagaratna et al. (2015). The contributions of organonitrates  
157 and organosulfates, detected as inorganic nitrate or sulfate ions by the AMS, to the elemental  
158 ratios were negligible because of their low mass concentrations (cf. Sect. A of the Supplement).  
159 Positive-matrix factorization (PMF) (Paatero and Tapper, 1994) was conducted on the organic  
160 mass spectra of the medium-resolution “V-mode” data ( $m/z$  12 to 220) taken to unit-mass  
161 resolution. The analysis used the PMF evaluation panel of Ulbrich et al. (2009) (version 4.2;



185 “robust mode”). Further aspects of the analysis and output evaluation are provided in Sect. C of  
186 the Supplement. Because of the low mass concentrations, the signal-to-noise ratios were  
187 insufficient for satisfactory PMF analysis of the high-resolution data. PMF results are reported  
188 herein for unit mass resolution.

189 The AMS mass spectra of SOM produced in the Harvard Environmental Chamber (HEC)  
190 by (i) the photooxidation of isoprene ( $C_5H_8$ ), (ii) the dark ozonolysis of the monoterpene  $\alpha$ -  
191 pinene ( $C_{10}H_{16}$ ) (adapted from Shilling et al. (2009)), and (iii) the dark ozonolysis of the  
192 sesquiterpene  $\beta$ -caryophyllene ( $C_{15}H_{24}$ ) are reported herein for the purpose of comparison to the  
193 AMAZE-08 data. Experimental details are described elsewhere (Shilling et al., 2009; King et al.,  
194 2010; Chen et al., 2011 and 2012). A library of spectra was collected at different SOM mass  
195 concentrations.

## 196 **33. Results and Discussion**

### 197 3.1 Mass concentrations

198 Figure 1 shows a time series of measurements by the AMS and other instruments during  
199 AMAZE-08. The AMS detects the non-refractory chemical components of the submicron  
200 fraction of the ambient particle population (NR-PM<sub>1</sub>) (Fig. 1a-1c). As described in Chen et al.  
201 (2009), organic material and sulfate were the two major components identified by the AMS,  
202 with correspondingly low concentrations of ammonium and negligible concentrations of nitrate  
203 and chloride. The campaign-average organic particle mass concentration was  $0.76 \pm 0.23 \mu\text{g m}^{-3}$ ,  
204 corresponding to  $0.45 \pm 0.13 \mu\text{g C m}^{-3}$  of organic carbon and an OM:OC ratio of 1.7. The  
205 campaign-average sulfate mass concentration of  $0.19 \pm 0.06 \mu\text{g m}^{-3}$  agreed well with the average  
206 value of  $0.21 \pm 0.06 \mu\text{g m}^{-3}$  measured by ion chromatography (IC) and the value of  $0.24 \pm 0.05$   
207  $\mu\text{g m}^{-3}$  measured by particle-induced X-ray emission (PIXE) for the fine-mode (PM<sub>2</sub>) filters.

208 Ammonium accounted for 2% of the submicron particle mass concentration. The campaign-  
209 average mass concentration was  $0.03 \pm 0.01 \mu\text{g m}^{-3}$ , in agreement with the average value of  $0.04$   
210  $\pm 0.01 \mu\text{g m}^{-3}$  obtained for the fine-mode filters by the IC analysis. Chloride concentrations, had  
211 a campaign-average concentration of  $2 \text{ ng m}^{-3}$ , which was consistent with the filter average,  
212 though there were transiently larger levels (up to  $26 \text{ ng m}^{-3}$ ) during some periods. Nitrate had a  
213 campaign-average concentration of  $7 \pm 2 \text{ ng m}^{-3}$ . This value was greater than the average fine-  
214 mode concentration of  $4 \pm 1 \text{ ng m}^{-3}$  measured by IC, perhaps because of increased instrument  
215 uncertainties at low concentrations. Another possibility, meaning substantial evaporative losses  
216 of nitrate during filter sampling, is not anticipated for the hygroscopic, acidic particles present  
217 during the measurement periods for the prevailing relative humidity. The AMS-measured nitrate  
218 accounted for 0.6% of the total submicron particle mass concentration.

219 Black carbon, mineral dust, and sea salt are common refractory components that are not  
220 quantified by the AMS. The multiangle absorption photometer (MAAP) instrument provides an  
221 optically based measurement of the black-carbon-equivalent (BCe) mass concentration, without  
222 size resolution (Petzold et al., 2002). The campaign-average concentration was  $0.13 \mu\text{g m}^{-3}$  (Fig.  
223 1d). Under a limiting assumption that all black carbon occurred in the submicron fraction of the  
224 atmospheric particle population, this concentration corresponded to 11% of the submicron mass  
225 concentration (inset of Fig. 1e). The relative contribution of black carbon varied significantly  
226 during the course of AMAZE-08 (Fig. 1e), perhaps corresponding to the occasional advection of  
227 urban pollution from Manaus or biomass burning from Africa (Kuhn et al., 2010; Martin et al.,  
228 2010b; Rizzo et al., 2013). This interpretation is supported by the covariance of BCe with  
229 sulfate. Major fine-mode ( $\text{PM}_2$ ) trace elements of mineral dust, including Si, Al, Fe, and Ca, had  
230 campaign-average mass concentrations of 0.12, 0.05, 0.04, and  $0.01 \mu\text{g m}^{-3}$ , respectively, as

231 analyzed for fine-mode filter samples by PIXE. An important source of the mineral dust was  
232 long-range transport from Africa. Previous campaigns in the Amazon found that about 20% of  
233 the mineral dust occurred in the submicron domain (Fuzzi et al., 2007). Using this result for  
234 AMAZE-08 implies that mineral dust contributed about  $0.1 \mu\text{g m}^{-3}$  to the average mass  
235 concentration of the submicron particle population (Malm et al., 1994). The modified pie chart is  
236 shown in Fig. S2. Moreover, the campaign-average mass concentrations of fine-mode metallic  
237 elements (V, Cr, Mn, Ni, Cu, Zn, Pb, and Mg in total of  $2 \text{ ng m}^{-3}$ ) measured by PIXE were  
238 sufficiently low during AMAZE-08 to confirm the absence in the submicron particle mass  
239 concentration of significant metals from anthropogenic sources. The campaign-average mass  
240 concentration of fine-mode  $\text{Na}^+$  measured by IC was  $0.02 \mu\text{g m}^{-3}$ . This result suggests a minimal  
241 contribution of sea salt from [the](#) Atlantic Ocean, at least to the submicron particle population  
242 (Fuzzi et al., 2007).

243 Figure 1f shows the time series of the particle light scattering coefficient measured by  
244 nephelometry at 550 nm for  $\text{PM}_{7.5}$ . The elevated scattering coefficients during 22 February to 3  
245 March 2008 were driven by elevated mineral dust concentrations in the coarse mode, along with  
246 elevated submicron sulfate, BCo, and organic material arising from the advection of the Manaus  
247 pollution plume as well as long-range transport from Africa (Sect. B of the Supplement). Other  
248 temporal maxima corresponded to increases of submicron particle mass concentration. Figure 1g  
249 shows the elemental compositions of the submicron organic material measured by the AMS. The  
250 O:C and H:C ratios, corrected as described in Canagaratna et al. (2015), were  $0.58 \pm 0.16$  (one  
251 standard deviation) and  $1.60 \pm 0.18$ , on average, respectively. The 10/90 quantiles were  
252 0.40/0.74 and 1.42/1.80, respectively. The N:C ratios were  $0.03 \pm 0.01$ .

253 Ammonium and sulfate mass concentrations had high correlation ( $R^2 = 0.95$ ) during

254 AMAZE-08 (Fig. S3). The molar ratio of  $\text{NH}_4^+ : \text{SO}_4^{2-}$  was 0.80 (Fig. 2), meaning that there was  
255 insufficient ammonium to neutralize sulfate for the submicron particle population and suggesting  
256 a composition close to that of ammonium bisulfate. Similar molar ratios have been reported in  
257 several previous studies in the central and northeast Amazon basin (Talbot et al., 1988, 1990;  
258 Gerab et al., 1998; Graham et al., 2003b). The AMS is unable to quantify refractory components  
259 such as  $\text{K}^+$ ,  $\text{Na}^+$ ,  $\text{Ca}^{2+}$ , and  $\text{Mg}^{2+}$ . Mass-diameter distributions of these ions obtained by IC  
260 analysis of samples collected by a Multi-Orifice Uniform Deposit Impactor (MOUDI) on 22  
261 March 2008 suggest that 40% of the mass of these ions was distributed to the submicron particle  
262 fraction. For comparison, Fuzzi et al. (2007) for the wet season reported 50-60% of  $\text{K}^+$  and  $\text{Ca}^{2+}$   
263 in the submicron fraction, compared to the predominance of  $\text{Na}^+$  and  $\text{Mg}^{2+}$  in the supermicron  
264 fraction. The campaign-average fine-mode mass concentrations of  $\text{K}^+$ ,  $\text{Ca}^{2+}$ ,  $\text{Na}^+$ , and  $\text{Mg}^{2+}$   
265 measured by IC were 0.03, 0.01, 0.02, and 0.01  $\mu\text{g m}^{-3}$ , respectively. The implication of the  
266 relative concentrations (i.e., sulfate concentration of  $0.19 \pm 0.06 \mu\text{g m}^{-3}$ ) is that the submicron  
267 inorganic ion composition is reasonably approximated as ammonium bisulfate during AMAZE-  
268 08.

269         Diel profiles of organic, sulfate, ammonium, nitrate, and chloride mass concentrations  
270 measured by the AMS are shown in Fig. 3. The temporal trends of the four species were  
271 correlated, with a minimum in mass concentrations near daybreak and a maximum in the  
272 afternoon. Nighttime rainfall efficiently removed particle mass concentration after local midnight,  
273 suggesting an absence of strong sources of submicron particles during the night. From the  
274 morning to the afternoon, photochemical production of SOM, convective mixing of particles  
275 from aloft, and regional advection sustained mass concentrations, with quick recovery after  
276 daytime rainfall. Precipitation was typically local whereas advection was typically regional at a

277 larger scale than precipitation. The decrease and the recovery of species concentration during the  
278 afternoon resulted from frequent rain events around that time of day (e.g., Fig. S4). The organic  
279 particle mass concentration increased during the day even as temperature rose and relative  
280 humidity dropped, both of which provide a thermodynamic driving force for the re-partitioning  
281 of semivolatile species from the particle phase to the gas phase (Pankow, 1994). Possible  
282 explanations include (1) sufficiently strong daytime production of SOM to outweigh evaporative  
283 sinks, (2) significant production of low-volatility SOM (Ervens et al., 2011; Ehn et al., 2014), or  
284 (3) a slow evaporation rate of SOM (Vaden et al., 2011).

### 285 3.2. Mass spectra of laboratory biogenic SOM

286 As a reference for interpreting the AMAZE-08 measurements, Figure 4 shows the mass  
287 spectra of SOM produced in the HEC by the oxidation of isoprene,  $\alpha$ -pinene, and  $\beta$ -  
288 caryophyllene for three different mass concentrations. Signals at  $m/z < 60$  account for 93-97%,  
289 80-84%, and 71-79% of the total signal intensity for the three types of SOM. The fragmentation  
290 pattern extends to higher  $m/z$  for the increasing carbon skeleton of precursor BVOC. For all three  
291 types of SOM, the relative intensities of two prominent ions,  $C_2H_3O^+$  at  $m/z$  43 and  $CO_2^+$  at  $m/z$   
292 44, show opposite trends as the mass concentration increases. The former increases for elevated  
293 concentrations whereas the later decreases. Another ion at  $m/z$  44,  $C_2H_4O^+$ , shows a trend  
294 similar to that of  $C_2H_3O^+$ . This ion accounts for 10–25%, 3–5%, and 5–10% of the signal at  $m/z$   
295 44 for the isoprene,  $\alpha$ -pinene, and  $\beta$ -caryophyllenethe SOMs, respectively. The relative  
296 intensities of major  $C_xH_y^+$  ions, such as  $CH_3^+$  at  $m/z$  15,  $C_2H_3^+$  at  $m/z$  27,  $C_3H_3^+$  at  $m/z$  39, and  
297  $C_3H_5^+$  at  $m/z$  41, typically increase as concentration increases. The most intense  $C_xH_y^+$  ions at  $m/z >$   
298 80 for the three types of biogenic SOM is  $C_7H_7^+$  at  $m/z$  91, which does not occur in the spectra for  
299 fresh emissions such as diesel exhaust, cooking, and biomass burning but is similar to the spectra

300 for aged primary emissions (Chirico et al., 2010; He et al., 2010; Ortega et al., 2013).

301 Compared to the spectra of the other types of biogenic SOM, isoprene-derived SOM  
302 under HO<sub>2</sub>-dominant conditions has a unique signature. “HO<sub>2</sub>-dominant” refers to the fate of  
303 peroxy radicals with respect to reaction with HO<sub>2</sub> or NO. The relative intensities of CHO<sup>+</sup> at *m/z*  
304 29, CH<sub>2</sub>O<sup>+</sup> at *m/z* 30, CH<sub>3</sub>O<sup>+</sup> at *m/z* 31, C<sub>3</sub>H<sub>6</sub>O<sub>2</sub><sup>+</sup> at *m/z* 74, and C<sub>3</sub>H<sub>7</sub>O<sub>2</sub><sup>+</sup> at *m/z* 75 in the spectra  
305 of isoprene-derived SOM are much greater, and the contributions of C<sub>x</sub>H<sub>y</sub><sup>+</sup> ions are less,  
306 especially for *m/z* > 65. Moreover, *m/z* 82 that mainly consists of C<sub>3</sub>H<sub>5</sub>O<sup>+</sup> appears to be the most  
307 intense peak for *m/z* ≥ 75. This fragment has been suggested as a characteristic fragment of  
308 isoprene-derived SOM (Robinson et al., 2011). Isoprene-derived SOM also does not follow the  
309 empirical linear relationship between O:C and *I*<sub>44</sub>:*I*<sub>org</sub> described by Aiken et al. (2008) (Fig. S5),  
310 indicating that deriving O:C from *I*<sub>44</sub>:*I*<sub>org</sub> requires careful judgments on the contribution of  
311 isoprene-derived SOM.

### 312 3.3 Multivariate factor analysis of the organic mass spectra

313 Multivariate analysis by PMF of the temporal series of the organic component of the  
314 mass spectra was carried out for 12 ≤ *m/z* ≤ 220 at unit-mass resolution. In overview, four  
315 statistical factors were identified and labeled as HOA, OOA-1, OOA-2, and OOA-3 (Fig. 5).  
316 These four factors respectively accounted for 2%, 18%, 14%, and 66% of the variance in the data  
317 matrix, with a residual variance of <1%. The time series of the loading of each statistical factor  
318 are shown in Fig. 6. By definition, the mass spectrum of the organic chemical component itself  
319 was at any time point a linear mix of the statistical factors, plus residual.

320 The HOA factor (Fig. 5a) was dominated by the ion series C<sub>n</sub>H<sub>2n+1</sub><sup>+</sup>, C<sub>n</sub>H<sub>2n-1</sub><sup>+</sup>, and C<sub>n</sub>H<sub>2n-3</sub><sup>+</sup>  
321 (*m/z* 27, 29, 39, 41, 43, 55, 57, 67, 69...), similar to that reported for other locations (e.g., Zhang  
322 et al., 2005; Docherty et al., 2011; Robinson et al., 2011) and to that observed for engine exhaust

323 (Canagaratna et al., 2004; Chirico et al., 2010). This statistical factor is typically taken as an  
324 organic component associated with fossil fuel combustion emissions that have not undergone  
325 substantial atmospheric oxidation. This factor was especially prevalent in the early part of the  
326 experiment. During this time period, other pollution tracers such as sulfate and NO<sub>x</sub> were also at  
327 elevated concentrations. Regional pollution from Manaus and local emissions (e.g., nearby roads,  
328 highway, generator, and pump oil) were plausible contributors to the loading of the HOA factor  
329 (Ahlm et al., 2009; Rizzo et al., 2013).

330 The factors OOA-1, OOA-2, and OOA-3 were ranked by the  $f_{44}:f_{43}$  ratios (high to low)  
331 and labeled based on Zhang et al. (2011), where  $f_{m/z}$  represents the fractional contribution of the  
332 signal intensity at  $m/z$  to the statistical factor. The signal intensity was dominated at  $m/z$  44 by  
333 the CO<sub>2</sub><sup>+</sup> fragment and at  $m/z$  43 by the C<sub>2</sub>H<sub>3</sub>O<sup>+</sup> and C<sub>3</sub>H<sub>7</sub><sup>+</sup> fragments. The  $f_{44}:f_{43}$  ratio has been  
334 used in some settings as a surrogate for the extent of oxidation (i.e., so-called ‘atmospheric  
335 aging’) of SOM (Ng et al., 2010 and 2011).

336 The OOA-1 factor had the feature of a singularly dominant peak at  $m/z$  44 (Fig. 5b). This  
337 marker has been linked to organic material that has undergone extensive oxidation during a  
338 prolonged atmospheric residence time (on the order of 10 days) (Ng et al., 2010; Lambe et al.,  
339 2011). This factor is consistent with an association to finding of highly-oxidized organic material  
340 delivered by long-range transport, as occurred during some periods of AMAZE-08 (Chen et al.,  
341 2009). The source of this material was plausibly African biomass burning, as supported by  
342 concurrent lidar measurements (Baars et al., 2011) and satellite observations (Ben-Ami et al.,  
343 2010). Biomass burning in South America was much less significant during the wet season  
344 (Martin et al., 2010b). The correlations of the statistical loadings of the OOA-1 factor with the  
345 measured mass concentrations of biomass burning tracers, such as chloride ( $R^2 = 0.52$ ),

346 potassium ( $R^2 = 0.35$ ), and black carbon ( $R^2 = 0.43$ ) in the submicron particle population, were  
347 not high, possibly because of the mixing of sources to these tracers such as primary biological  
348 particles (i.e., contributing chloride and potassium) and regional pollution from Manaus to (i.e.,  
349 black carbon). These correlation values were, however, significantly greater than those of the  
350 other three factors (HOA, OOA2, and OOA-3) with the tracers (i.e.,  $R^2 < 0.10$  for chloride,  $R^2 <$   
351  $0.02$  for potassium, and  $R^2 < 0.20$  for black carbon) (Fig. 6b). Elevated sulfate mass  
352 concentrations were also observed during periods having high OOA-1 loadings (Fig. 1b).

353 Features of the OOA-2 factor included (1) a  $f_{44}:f_{43}$  ratio greater than unity and (2) a  
354 characteristic peak at  $m/z$  82 mainly consisting of  $C_3H_5O^+$ . This peak was the most abundant for  
355  $m/z \geq 75$  (Fig. 5c). It is similar to that reported for PMF factors identified in the tropical  
356 rainforest of Borneo (named as the “82Fac” factor) (Robinson et al., 2011), the rural area of  
357 southwest Ontario, Canada (named as the “UNKN” factor) (Slowik et al., 2011), and isoprene-  
358 rich downtown Atlanta, Georgia, USA (named as the “IEPOX-OA” factor) (Budisulistiorini et  
359 al., 2013). Robinson et al. (2011) concluded that this factor derived from SOM produced by  
360 isoprene photo-oxidation. In agreement, the time series of OOA-2 loading correlated with  
361 isoprene concentration ( $R^2 = 0.65$ ) as well as with the sum concentration of first-generation  
362 isoprene oxidation products, specifically MVK + MACR ( $R^2 = 0.74$ ) (Fig. 6c). The characteristic  
363  $m/z$  82 also occurred in the spectra of our isoprene SOM produced in the presence of neutral  
364 sulfate particles at 40% RH (Fig. 4a). Laboratory studies demonstrated that the reactive-uptake  
365 of photo-oxidation products of isoprene, particularly IEPOX, in the presence of acidic particles  
366 contribute to the  $m/z$  82 signal detected by the AMS (Lin et al., 2012; Budisulistiorini et al.,  
367 2013; Liu et al., 2014). Even so, the spectra of isoprene SOM or IEPOX SOM produced in the  
368 laboratory have some important differences with the statistical factories-factors (i.e., “OOA-2” of



369 this study and “82Fac”, “UNKN”, and “IEPOX-OA” of earlier studies) derived from  
370 atmospheric data sets. In particular, there are significant differences at  $m/z$  29 and  $m/z$  39 through  
371  $m/z$  44. The values of  $f_{44}$  of the laboratory results are approximately 25% of those of the cited  
372 PMF factors. One possible explanation for these differences is that the laboratory experiments  
373 did not capture the full range of atmospheric processes, such as possible synergistic chemistry  
374 among the range of atmospheric precursors, aqueous-phase processing, and photochemistry  
375 under a range of  $\text{HO}_2$ :NO ratios (Ervens et al., 2011; Emanuelsson et al., 2013; Liu et al., 2013;  
376 Nguyen et al., 2014). In particular, the laboratory experiments were typically carried out at low  
377 relative humidity. The atmosphere during AMAZE-08 was humid (89 to 100% RH; 25 to 75%  
378 quantiles). Pöhlker et al. (2012) showed evidence of multiphase processing in the larger  
379 accumulation mode particles. The oxidized material produced by aqueous-phase oxidation (e.g.,  
380 dicarboxylic acids (Lim et al., 2010)) may explain the higher  $f_{44}$  in the OOA-2 factor compared  
381 to the laboratory spectra. In summary, the OOA-2 factor during AMAZE-08 was interpreted as  
382 SOM produced by the reactive uptake of isoprene photo-oxidation products, including possible  
383 aqueous-phase oxidation in haze, fog, and cloud droplets.

384 The OOA-3 factor had a prominent peak at  $m/z$  43 (Fig. 5d). For  $m/z > 80$ , the most  
385 intense peak occurred at  $m/z$  91. The OOA-3 factor had similarities to the mass spectra recorded  
386 for biogenic SOM produced under conditions relevant to the Amazon basin. Specifically, SOM  
387 produced from isoprene under laboratory conditions had a prominent peak at  $m/z$  43 (Fig. 4a).  
388 Mass spectra of SOM derived from precursors of monoterpene  $\alpha$ -pinene and sesquiterpene  $\beta$ -  
389 caryophyllene had similar patterns as OOA-3 at  $m/z$  55 and  $m/z$  91. A linear combination of the  
390 three chamber spectra largely reproduced the OOA-3 factor (Fig. 7; 50% isoprene-derived SOM,  
391 30%  $\alpha$ -pinene-derived SOM, and 20%  $\beta$ -caryophyllene-derived SOM). The intensity at  $m/z$  29,

392 however, was overestimated by the linear combination. The remarkable result is that the ambient  
393 factor could to large extent be explained by just three laboratory data sets given the wide range  
394 of BVOC precursor compounds that can contribute to SOM production in the Amazon basin.  
395 The explanation is three-fold, one that isoprene is the dominant BVOC for this rain forest, two  
396 that the AMS breaks complex molecules into simpler building blocks by electron-impact  
397 ionization, and three that the higher-order C<sub>10</sub>, C<sub>15</sub>, and possibly C<sub>20</sub> BVOCs are all assembled  
398 biochemically from the isoprene (C<sub>5</sub>) monomer. Moreover, the temporal variation of the OOA-3  
399 loading tracked that of the BVOC concentrations (Fig. 6d). The OOA-3 statistical factor was  
400 therefore interpreted as associated with freshly produced SOM similar to that produced in the  
401 chamber experiments, meaning on a timescale of several hours by a mechanism of gas-to-particle  
402 partitioning of the BVOC oxidation products.

403         Figure 8 shows the campaign-average diel profiles of the factor loadings. The HOA  
404 loading had a daytime minimum, suggesting the buildup of local pollution during the night and  
405 the removal by convective mixing during the day. In support of this interpretation, the nocturnal  
406 boundary layer was approximately 100 m or less. At daybreak, the boundary layer rapidly  
407 developed, reaching on order of 1000 m by local noon around the site (Martin et al., 2010b). The  
408 OOA-1 loading peaked around noon without great variation throughout the day. This temporal  
409 behavior is expected for homogeneous mixing in the atmospheric column without in situ sources,  
410 such as for material arriving by long-range transport. The small daytime increase was consistent  
411 with the daytime convective downward mixing of older, oxidized particles from aloft. By  
412 comparison, the OOA-2 and OOA-3 loadings peaked in the early afternoon while the BVOC  
413 concentrations were high (cf. Fig. 3c of Chen et al. (2009)). This temporal behavior was  
414 consistent with the photochemically driven production of SOM.

415 Figure 9 shows the time series of fractional contribution by each of the four statistical  
416 factors identified by PMF analysis. On average the relative loadings of HOA, OOA-1, OOA-2,  
417 and OOA-3 were 14%, 14%, 34%, and 38%, respectively. For comparison, other studies reported  
418 0 to 21% of HOA for remote locations (Jimenez et al., 2009) and 23% to 50% of OOA-2 (named  
419 as “82Fac”, “UNKN”, and “IEPOX-OA” in earlier studies) (Robinson et al., 2011; Slowik et al.,  
420 2011; Budisulistiorini et al., 2013). Figure 9 shows that the relative importance of each process  
421 as a contributor differed with time and highlights two focus periods. Precipitation and  
422 temperature were the major meteorological factors that differed between the two periods. The  
423 first period was sunny, warmer with occasional clouds, and the second period had frequent heavy  
424 rainfall events. Long-range back-trajectory analyses presented in Martin et al. (2010b) showed  
425 that the air masses consistently arrived from the equatorial Atlantic Ocean passing as  
426 northeasterlies through the Amazon basin. Local measurements showed that the daytime winds  
427 mainly came from the north and northeast (Fig. 9, top). During the first period, the average  
428 fractional contribution by the OOA-2 factor was five times greater than that of the OOA-3 factor.  
429 During the second period, by comparison, the fractional contribution by the OOA-3 factor was  
430 three times greater than that of the OOA-2 factor. The average organic mass concentrations of  
431 the two periods were 1.84 and 0.59  $\mu\text{g m}^{-3}$ , respectively.

432 Figure 9 shows that the loading fraction of the OOA-2 factor consistently dropped  
433 following heavy rainfall events, suggesting more efficient in-cloud or below-cloud scavenging  
434 for the types of material represented by OOA-2 than for those types represented by OOA-3. This  
435 finding further supports the interpretation that the OOA-2 factor represents, at least in part,  
436 aqueous-phase production pathways because SOM produced in this way has greater water  
437 solubility and hence greater wet deposition rates than SOM produced freshly by gas-to-particle

461 condensation, as interpreted for the OOA-3 factor. Figure 9 also shows that the mode diameter of  
462 organic material in period 1, which has a higher OOA-2 loading fraction, is significantly larger  
463 than that in period 2, which has a higher OOA-3 loading fraction. Aqueous-phase processing is  
464 anticipated to add additional organic material that results in larger mode diameters after  
465 dehydration.

#### 466 **4.4. Conclusions**

467 Submicron particle mass concentration in the Amazonian rainforest during the wet season  
468 of 2008 was dominated by organic material. The environment was humid, HO<sub>2</sub>-dominant,  
469 isoprene-rich, with the presence of acidic particles in the submicron fraction of the atmospheric  
470 particle population. Factors OOA-2 and OOA-3 were identified in the patterns of the collected  
471 mass spectra. These factors were interpreted as tied to the in-basin production of biogenic  
472 secondary organic material and together accounted for >70% of the factor loadings, with the  
473 balance from HOA and OOA-1. The OOA-2 factor was implicated as associated with the  
474 reactive uptake of isoprene oxidation products, especially of epoxydiols to acidic haze, fog or  
475 cloud droplets. The OOA-3 factor was consistent with an association to the fresh production of  
476 SOM by a mechanism of gas-phase oxidation of BVOCs followed by gas-to-particle conversion  
477 of the oxidation products. Although multivariate statistical factors do not correspond to  
478 segregated individual chemical components (e.g., unlike molecules or families of molecules), the  
479 factors nevertheless can be indicative of the relative importance of different atmospheric  
480 emissions and process pathways. With this caveat in mind, the PMF analysis herein finds that the  
481 factor loadings were, on average, in a ratio of 1.4:1 for OOA-2 compared to OOA-3 and were  
482 alternately dominated in different periods of AMAZE-08 by the OOA-2 and OOA-3. These  
483 findings suggest a comparable importance of gas-phase and particle-phase (including haze, fog,

Formatted  
or grammar

484 and cloud droplets) production of SOM during the study period.

**Acknowledgments.** Support was received from the USA National Science Foundation, the German Max Planck Society, and Brazilian CNPq and FAPESP agencies. QC acknowledges a NASA Earth and Space Science Fellowship. DKF acknowledges a NOAA Global Change Fellowship. TP acknowledges the CNPq grant 552831/2006-9. PA acknowledges FAPESP projects 2008/58100-2, 2010/52658-1, 2011/50170-4, 2012/14437-9. We thank the INPA LBA central office in Manaus for logistical support during AMAZE-08. We thank John Jayne, Joel Kimmel, Johannes Schneider, and Soeren Zorn for helping with sampling and aspects of data analysis.

## References

Ahlm, L., Nilsson, E. D., Krejci, R., Martensson, E. M., Vogt, M., and Artaxo, P.: Aerosol number fluxes over the Amazon rain forest during the wet season, *Atmos. Chem. Phys.*, 9, 9381-9400, 2009.

Aiken, A. C., Decarlo, P. F., Kroll, J. H., Worsnop, D. R., Huffman, J. A., Docherty, K. S., Ulbrich, I. M., Mohr, C., Kimmel, J. R., Sueper, D., Sun, Y., Zhang, Q., Trimborn, A., Northway, M., Ziemann, P. J., Canagaratna, M. R., Onasch, T. B., Alfarra, M. R., Prevot, A. S. H., Dommen, J., Duplissy, J., Metzger, A., Baltensperger, U., and Jimenez, J. L.: O/C and OM/OC ratios of primary, secondary, and ambient organic aerosols with high-resolution time-of-flight aerosol mass spectrometry, *Environ. Sci. Technol.*, 42, 4478-4485, 10.1021/es703009q, 2008.

~~[Andreae, M. O.: Aerosols before pollution, \*Science\*, 315, 50-51, 10.1126/science.1136529, 2007.](#)~~

Andreae, M. O., Berresheim, H., Bingemer, H., Jacob, D. J., Lewis, B. L., Li, S. M., and Talbot, R. W.: The atmospheric sulfur cycle over the Amazon Basin. 2. Wet season, *J. Geophys. Res.*, 95, 16813-16824, 1990.

~~[Andreae, M. O.: Aerosols before pollution, \*Science\*, 315, 50-51, 10.1126/science.1136529, 2007.](#)~~

Baars, H., Ansmann, A., Althausen, D., Engelmann, R., Artaxo, P., Pauliquevis, T., and Souza, R.: Further evidence for significant smoke transport from Africa to Amazonia, *Geophys. Res. Lett.*, 38, L20802, 10.1029/2011GL049200, 2011.

Ben-Ami, Y., Koren, I., Rudich, Y., Artaxo, P., Martin, S. T., and Andreae, M. O.: Transport of North African dust from the Bodele depression to the Amazon Basin: a case study, *Atmos. Chem. Phys.*, 10, 7533-7544, 10.5194/acp-10-7533-2010, 2010.

Budisulistiorini, S. H., Canagaratna, M. R., Croteau, P. L., Marth, W. J., Baumann, K., Edgerton, E. S., Shaw, S. L., Knipping, E. M., Worsnop, D. R., Jayne, J. T., Gold, A., and Surratt, J. D.: Real-time continuous characterization of secondary organic aerosol derived from isoprene epoxydiols in downtown Atlanta, Georgia, using the Aerodyne aerosol chemical speciation monitor, *Environ. Sci. Technol.*, 47, 5686-5694, 10.1021/es400023n, 2013.

Canagaratna, M. R., Jayne, J. T., Ghertner, D. A., Herndon, S., Shi, Q., Jimenez, J. L., Silva, P. J., Williams, P., Lanni, T., Drewnick, F., Demerjian, K. L., Kolb, C. E., and Worsnop, D. R.: Chase studies of particulate emissions from in-use New York City vehicles, *Aerosol Sci. Technol.*, 38, 555-573, Doi 10.1080/02786820490465504, 2004.

Canagaratna, M. R., Jimenez, J. L., Kroll, J. H., Chen, Q., Kessler, S. H., Massoli, P., Hildebrandt Ruiz, L., Fortner, E., Williams, L. R., Wilson, K. R., Surratt, J. D., Donahue, N. M., Jayne, J. T., and Worsnop, D. R.: Elemental ratio measurements of organic compounds using aerosol mass spectrometry: characterization, improved calibration, and implications, *Atmos. Chem. Phys.*, 15, 253-272, 10.5194/acp-15-253-2015, 2015.

Chen, Q., Farmer, D. K., Schneider, J., Zorn, S. R., Heald, C. L., Karl, T. G., Guenther, A., Allan, J. D., Robinson, N., Coe, H., Kimmel, J. R., Pauliquevis, T., Borrmann, S., [Pöschl, U.](#), Andreae, M. O., Artaxo, P., Jimenez, J. L., and Martin, S. T.: Mass spectral characterization of submicron biogenic organic particles in the Amazon Basin, *Geophys. Res. Lett.*, 36, L20806, 10.1029/2009gl039880, 2009.

Chen, Q., Liu, Y., Donahue, N. M., Shilling, J. E., and Martin, S. T.: Particle-phase chemistry of secondary organic material: Modeled compared to measured O:C and H:C elemental ratios provide constraints, *Environ. Sci. Technol.*, 45, 4763-4770, 10.1021/es104398s, 2011.

Chen, Q., Li, Y. L., McKinney, K. A., Kuwata, M., and Martin, S. T.: Particle mass yield from  $\beta$ -caryophyllene ozonolysis, *Atmos. Chem. Phys.*, 12, 3165-3179, 10.5194/acp-12-3165-2012, 2012.

Chirico, R., DeCarlo, P. F., Heringa, M. F., Tritscher, T., Richter, R., Prevot, A. S. H., Dommen, J., Weingartner, E., Wehrle, G., Gysel, M., Laborde, M., and Baltensperger, U.: Impact of aftertreatment devices on primary emissions and secondary organic aerosol formation potential from in-use diesel vehicles: results from smog chamber experiments, *Atmos. Chem. Phys.*, 10, 11545-11563, 10.5194/acp-10-11545-2010, 2010.

Docherty, K. S., Aiken, A. C., Huffman, J. A., Ulbrich, I. M., DeCarlo, P. F., Sueper, D., Worsnop, D. R., Snyder, D. C., Peltier, R. E., Weber, R. J., Grover, B. D., Eatough, D. J., Williams, B. J., Goldstein, A. H., Ziemann, P. J., and Jimenez, J. L.: The 2005 Study of Organic Aerosols at Riverside (SOAR-1): instrumental intercomparisons and fine particle composition, *Atmos. Chem. Phys.*, 11, 12387-12420, 10.5194/acp-11-12387-2011, 2011.

Ehn, M., Thornton, J. A., Kleist, E., Sipila, M., Junninen, H., Pullinen, I., Springer, M., Rubach, F., Tillmann, R., Lee, B., Lopez-Hilfiker, F., Andres, S., Acir, I. H., Rissanen, M., Jokinen, T., Schobesberger, S., Kangasluoma, J., Kontkanen, J., Nieminen, T., Kurten, T., Nielsen, L. B., Jorgensen, S., Kjaergaard, H. G., Canagaratna, M., Dal Maso, M., Berndt, T., Petaja, T., Wahner, A., Kerminen, V. M., Kulmala, M., Worsnop, D. R., Wildt, J., and Mentel, T. F.: A large source of low-volatility secondary organic aerosol, *Nature*, 506, 476-479, 10.1038/nature13032, 2014.

Elbert, W., Taylor, P. E., Andreae, M. O., and Pöschl, U.: Contribution of fungi to primary biogenic aerosols in the atmosphere: wet and dry discharged spores, carbohydrates, and inorganic ions, *Atmos. Chem. Phys.*, 7, 4569-4588, 10.5194/acp-7-4569-2007, 2007.

Emanuelsson, E. U., Hallquist, M., Kristensen, K., Glasius, M., Bohn, B., Fuchs, H., Kammer, B., Kiendler-Scharr, A., Nehr, S., Rubach, F., Tillmann, R., Wahner, A., Wu, H. C., and Mentel, T. F.: Formation of anthropogenic secondary organic aerosol (SOA) and its influence on biogenic SOA properties, *Atmos. Chem. Phys.*, 13, 2837-2855, 10.5194/acp-13-2837-2013, 2013.

Ervens, B., Turpin, B. J., and Weber, R. J.: Secondary organic aerosol formation in cloud droplets and aqueous particles (aqSOA): a review of laboratory, field and model studies, *Atmos. Chem. Phys.*, 11, 11069-11102, 10.5194/acp-11-11069-2011, 2011.

Fuzzi, S., Decesari, S., Facchini, M. C., Cavalli, F., Emblico, L., Mircea, M., Andreae, M. O., Trebs, I., Hoffer, A., Guyon, P., Artaxo, P., Rizzo, L. V., Lara, L. L., Pauliquevis, T., Maenhaut, W., Raes, N., Chi, X. G., Mayol-Bracero, O. L., Soto-Garcia, L. L., Claeys, M., Kourtev, I., Rissler, J., Swietlicki, E., Tagliavini, E., Schkolnik, G., Falkovich, A. H., Rudich, Y., Fisch, G., and Gatti, L. V.: Overview of the inorganic and organic composition of size-segregated aerosol in Rondonia, Brazil, from the biomass-burning period to the onset of the wet season, *J. Geophys. Res.*, 112, D01201, 10.1029/2005JD006741, 2007.

Gerab, F., Artaxo, P., Gillett, R., and Ayers, G.: PIXE, PIGE and ion chromatography of aerosol particles from northeast Amazon Basin, *Nucl Instrum Meth B*, 136, 955-960, 1998.

Graham, B., Guyon, P., Taylor, P. E., Artaxo, P., Maenhaut, W., Glovsky, M. M., Flagan, R. C., and Andreae, M. O.: Organic compounds present in the natural Amazonian aerosol: Characterization by gas chromatography-mass spectrometry, *J. Geophys. Res.*, 108, 4766, 10.1029/2003jd003990, 2003a.

Graham, B., Guyon, P., Maenhaut, W., Taylor, P. E., Ebert, M., Matthias-Maser, S., Mayol-Bracero, O. L., Godoi, R. H. M., Artaxo, P., Meixner, F. X., Moura, M. A. L., Rocha, C., Van Grieken, R., Glovsky, M. M., Flagan, R. C., and Andreae, M. O.: Composition and diurnal variability of the natural Amazonian aerosol, *J. Geophys. Res.*, 108, 4765, 10.1029/2003JD004049, 2003b.

Gunthe, S. S., King, S. M., Rose, D., Chen, Q., Roldin, P., Farmer, D. K., Jimenez, J. L., Artaxo, P., Andreae, M. O., Martin, S. T., and Pöschl, U.: Cloud condensation nuclei in pristine tropical rainforest air of Amazonia: size-resolved measurements and modeling of atmospheric aerosol composition and CCN activity, *Atmos. Chem. Phys.*, 9, 7551-7575, 10.5194/acp-9-7551-2009, 2009.

He, L. Y., Lin, Y., Huang, X. F., Guo, S., Xue, L., Su, Q., Hu, M., Luan, S. J., and Zhang, Y. H.: Characterization of high-resolution aerosol mass spectra of primary organic aerosol emissions from Chinese cooking and biomass burning, *Atmos. Chem. Phys.*, 10, 11535-11543, DOI 10.5194/acp-10-11535-2010, 2010.

IPCC: *Climate Change 2013: The Physical Science Basis. Contribution of Working Group I to the Fifth Assessment Report of the Intergovernmental Panel on Climate Change* [Stocker, T.F., D. Qin, G.-K. Plattner, M. Tignor, S.K. Allen, J. Boschung, A. Nauels, Y. Xia, V. Bex and P.M. Midgley (eds.)], Cambridge University Press, Cambridge, United Kingdom and New York, NY, USA, 1535 pp, 2013.

Jimenez, J. L., Canagaratna, M. R., Donahue, N. M., Prevot, A. S. H., Zhang, Q., Kroll, J. H., DeCarlo, P. F., Allan, J. D., Coe, H., Ng, N. L., Aiken, A. C., Docherty, K. S., Ulbrich, I. M., Grieshop, A. P., Robinson, A. L., Duplissy, J., Smith, J. D., Wilson, K. R., Lanz, V. A., Hueglin, C., Sun, Y. L., Tian, J., Laaksonen, A., Raatikainen, T., Rautiainen, J., Vaattovaara, P., Ehn, M., Kulmala, M., Tomlinson, J. M., Collins, D. R., Cubison, M. J., Dunlea, E. J., Huffman, J. A., Onasch, T. B., Alfarra, M. R., Williams, P. I., Bower, K., Kondo, Y., Schneider, J., Drewnick, F., Borrmann, S., Weimer, S., Demerjian, K., Salcedo, D., Cottrell, L., Griffin, R., Takami, A., Miyoshi, T., Hatakeyama, S., Shimono, A., Sun, J. Y., Zhang, Y. M., Dzepina, K., Kimmel, J. R., Sueper, D., Jayne, J. T., Herndon, S. C., Trimborn, A. M., Williams, L. R., Wood, E. C., Middlebrook, A. M., Kolb, C. E., Baltensperger, U., and Worsnop, D. R.: Evolution of organic aerosols in the atmosphere, *Science*, 326, 1525-1529, 10.1126/science.1180353, 2009.

Karl, T., Guenther, A., Turnipseed, A., Tyndall, G., Artaxo, P., and Martin, S.: Rapid formation of isoprene photo-oxidation products observed in Amazonia, *Atmos. Chem. Phys.*, 9, 7753-7767, 2009.

King, S. M., Rosenoern, T., Shilling, J. E., Chen, Q., Wang, Z., Biskos, G., McKinney, K. A., ~~Pöschl~~ Pöschl, U., and Martin, S. T.: Cloud droplet activation of mixed organic-sulfate particles produced by the photooxidation of isoprene, *Atmos. Chem. Phys.*, 10, 3953-3964, 10.5194/acp-10-3953-2010, 2010.

Kuhn, U., Ganzeveld, L., Thielmann, A., Dindorf, T., Schebeske, G., Welling, M., Sciare, J., Roberts, G., Meixner, F. X., Kesselmeier, J., Lelieveld, J., Kolle, O., Ciccioli, P., Lloyd, J., Trentmann, J., Artaxo, P., and Andreae, M. O.: Impact of Manaus City on the Amazon Green Ocean atmosphere: ozone production, precursor sensitivity and aerosol load, *Atmos. Chem. Phys.*, 10, 9251-9282, 10.5194/acp-10-9251-2010, 2010.

Lambe, A. T., Onasch, T. B., Massoli, P., Croasdale, D. R., Wright, J. P., Ahern, A. T., Williams, L. R., Worsnop, D. R., Brune, W. H., and Davidovits, P.: Laboratory studies of the chemical composition and cloud condensation nuclei (CCN) activity of secondary organic aerosol (SOA) and oxidized primary organic aerosol (OPOA), *Atmos. Chem. Phys.*, 11, 8913-8928, 10.5194/acp-11-8913-2011, 2011.

Lim, Y. B., Tan, Y., Perri, M. J., Seitzinger, S. P., and Turpin, B. J.: Aqueous chemistry and its role in secondary organic aerosol (SOA) formation, *Atmos. Chem. Phys.*, 10, 10521-10539, 10.5194/acp-10-10521-2010, 2010.



Lin, Y. H., Zhang, Z. F., Docherty, K. S., Zhang, H. F., Budisulistiorini, S. H., Rubitschun, C. L., Shaw, S. L., Knipping, E. M., Edgerton, E. S., Kleindienst, T. E., Gold, A., and Surratt, J. D.: Isoprene epoxydiols as precursors to secondary organic aerosol formation: Acid-catalyzed reactive uptake studies with authentic compounds, *Environ. Sci. Technol.*, 46, 250-258, 10.1021/es202554c, 2012.

Liu, Y. J., Herdlinger-Blatt, I., McKinney, K. A., and Martin, S. T.: Production of methyl vinyl ketone and methacrolein via the hydroperoxyl pathway of isoprene oxidation, *Atmos. Chem. Phys.*, 13, 5715-5730, 10.5194/acp-13-5715-2013, 2013.

Liu, Y., Kuwata, M., Strick, B. F., Geiger, F. M., Thomson, R. J., McKinney, K. A., and Martin, S. T.: Uptake of epoxydiol isomers accounts for half of the particle-phase material produced from isoprene photooxidation via the HO<sub>2</sub> pathway, *Environ. Sci. Technol.*, 49, 250-258, 10.1021/es5034298, 2014.

Malm, W. C., Sisler, J. F., Huffman, D., Eldred, R. A., and Cahill, T. A.: Spatial and seasonal trends in particle concentration and optical extinction in the united states, *J. Geophys. Res.*, 99, 1347-1370, 1994.

Martin, S. T., Andreae, M. O., Artaxo, P., Baumgardner, D., Chen, Q., Goldstein, A. H., Guenther, A., Heald, C. L., Mayol-Bracero, O. L., McMurry, P. H., Pauliquevis, T., [Pöschl, U.](#), Prather, K. A., Roberts, G. C., Saleska, S. R., Dias, M. A. S., Spracklen, D. V., Swietlicki, E., and Trebs, I.: Sources and properties of amazonian aerosol particles, *Reviews of Geophysics*, 48, Rg2002, 10.1029/2008rg000280, 2010a.

Martin, S. T., Andreae, M. O., Althausen, D., Artaxo, P., Baars, H., Borrmann, S., Chen, Q., Farmer, D. K., Guenther, A., Gunthe, S. S., Jimenez, J. L., Karl, T., Longo, K., Manzi, A., [Müller, T.](#), Pauliquevis, T., Petters, M. D., Prenni, A. J., [Pöschl, U.](#), Rizzo, L. V., Schneider, J., Smith, J. N., Swietlicki, E., Tota, J., Wang, J., Wiedensohler, A., and Zorn, S. R.: An overview of the Amazonian Aerosol Characterization Experiment 2008 (AMAZE-08), *Atmos. Chem. Phys.*, 10, 11415-11438, 10.5194/acp-10-11415-2010, 2010b.

Matthew, B. M., Middlebrook, A. M., and Onasch, T. B.: Collection efficiencies in an Aerodyne aerosol mass spectrometer as a function of particle phase for laboratory generated aerosols, *Aerosol Sci. Technol.*, 42, 884-898, 10.1080/02786820802356797, 2008.

Ng, N. L., Canagaratna, M. R., Zhang, Q., Jimenez, J. L., Tian, J., Ulbrich, I. M., Kroll, J. H., Docherty, K. S., Chhabra, P. S., Bahreini, R., Murphy, S. M., Seinfeld, J. H., Hildebrandt, L., Donahue, N. M., DeCarlo, P. F., Lanz, V. A., Prevot, A. S. H., Dinar, E., Rudich, Y., and Worsnop, D. R.: Organic aerosol components observed in Northern Hemispheric datasets from Aerosol Mass Spectrometry, *Atmos. Chem. Phys.*, 10, 4625-4641, 10.5194/acp-10-4625-2010, 2010.

Ng, N. L., Canagaratna, M. R., Jimenez, J. L., Chhabra, P. S., Seinfeld, J. H., and Worsnop, D. R.: Changes in organic aerosol composition with aging inferred from aerosol mass spectra, *Atmos. Chem. Phys.*, 11, 6465-6474, 10.5194/acp-11-6465-2011, 2011.

Nguyen, T. B., Coggon, M. M., Bates, K. H., Zhang, X., Schwantes, R. H., Schilling, K. A., Loza, C. L., Flagan, R. C., Wennberg, P. O., and Seinfeld, J. H.: Organic aerosol formation from the reactive uptake of isoprene epoxydiols (IEPOX) onto non-acidified inorganic seeds, *Atmos. Chem. Phys.*, 14, 3497-3510, 10.5194/acp-14-3497-2014, 2014.

Ortega, A. M., Day, D. A., Cubison, M. J., Brune, W. H., Bon, D., de Gouw, J. A., and Jimenez, J. L.: Secondary organic aerosol formation and primary organic aerosol oxidation from biomass burning smoke in a flow reactor during FLAME-3, *Atmos. Chem. Phys.*, 13, 11551-11571, 10.5194/acp-13-11551-2013, 2013.

Paatero, P., and Tapper, U.: Positive matrix factorization - a nonnegative factor model with optimal utilization of error-estimates of data values, *Environmetrics*, 5, 111-126, 10.1002/env.3170050203, 1994.

Pankow, J. F.: An absorption-model of the gas aerosol partitioning involved in the formation of secondary organic aerosol, *Atmos. Environ.*, 28, 189-193, 1994.

Petzold, A., Kramer, H., and Schonlinner, M.: Continuous measurement of atmospheric black carbon using a multi-angle absorption photometer, *Environmental Science and Pollution Research*, 4, 78-82, 2002.

Pöhlker, C., Wiedemann, K. T., Sinha, B., Shiraiwa, M., Gunthe, S. S., Smith, M., Su, H., Artaxo, P., Chen, Q., Cheng, Y. F., Elbert, W., Gilles, M. K., Kilcoyne, A. L. D., Moffet, R. C., Weigand, M., Martin, S. T., Poeschl, U., and Andreae, M. O.: Biogenic potassium salt particles as seeds for secondary organic aerosol in the Amazon, *Science*, 337, 1075-1078, 10.1126/science.1223264, 2012.

Pöschl, U., Martin, S. T., Sinha, B., Chen, Q., Gunthe, S. S., Huffman, J. A., Borrmann, S., Farmer, D. K., Garland, R. M., Helas, G., Jimenez, J. L., King, S. M., Manzi, A., Mikhailov, E., Pauliquevis, T., Petters, M. D., Prenni, A. J., Roldin, P., Rose, D., Schneider, J., Su, H., Zorn, S. R., Artaxo, P., and Andreae, M. O.: Rainforest aerosols as biogenic nuclei of clouds and precipitation in the Amazon, *Science*, 329, 1513-1516, 10.1126/science.1191056, 2010.

Prenni, A. J., Petters, M. D., Kreidenweis, S. M., Heald, C. L., Martin, S. T., Artaxo, P., Garland, R. M., Wollny, A. G., and Pöschl, U.: Relative roles of biogenic emissions and Saharan dust as ice nuclei in the Amazon basin, *Nature Geoscience*, 2, 401-404, Doi 10.1038/Ngeo517, 2009.

Rizzo, L. V., Artaxo, P., Muller, T., Wiedensohler, A., Paixao, M., Cirino, G. G., Arana, A., Swietlicki, E., Roldin, P., Fors, E. O., Wiedemann, K. T., Leal, L. S. M., and Kulmala, M.: Long term measurements of aerosol optical properties at a primary forest site in Amazonia, *Atmos. Chem. Phys.*, 13, 2391-2413, 10.5194/acp-13-2391-2013, 2013.

Robinson, N. H., Hamilton, J. F., Allan, J. D., Langford, B., Oram, D. E., Chen, Q., Docherty, K., Farmer, D. K., Jimenez, J. L., Ward, M. W., Hewitt, C. N., Barley, M. H., Jenkin, M. E., Rickard, A. R., Martin, S. T., McFiggans, G., and Coe, H.: Evidence for a significant proportion of secondary organic aerosol from isoprene above a maritime tropical forest, *Atmos. Chem. Phys.*, 11, 1039-1050, 10.5194/acp-11-1039-2011, 2011.

- Schneider, J., Freutel, F., Zorn, S. R., Chen, Q., Farmer, D. K., Jimenez, J. L., Martin, S. T., Artaxo, P., Wiedensohler, A., and Borrmann, S.: Mass- spectrometric identification of primary biological particle markers and application to pristine submicron aerosol measurements in Amazonia, *Atmos. Chem. Phys.*, 11, 11415-11429, 10.5194/acp-11-11415-2011, 2011.
- Shilling, J. E., Chen, Q., King, S. M., Rosenoern, T., Kroll, J. H., Worsnop, D. R., DeCarlo, P. F., Aiken, A. C., Sueper, D., Jimenez, J. L., and Martin, S. T.: Loading-dependent elemental composition of  $\alpha$ -pinene SOA particles, *Atmos. Chem. Phys.*, 9, 771-782, 10.5194/acp-9-771-2009, 2009.
- Slowik, J. G., Brook, J., Chang, R. Y. W., Evans, G. J., Hayden, K., Jeong, C. H., Li, S. M., Liggi, J., Liu, P. S. K., McGuire, M., Mihele, C., Sjostedt, S., Vlasenko, A., and Abbatt, J. P. D.: Photochemical processing of organic aerosol at nearby continental sites: contrast between urban plumes and regional aerosol, *Atmos. Chem. Phys.*, 11, 2991-3006, DOI 10.5194/acp-11-2991-2011, 2011.
- Surratt, J. D., Chan, A. W. H., Eddingsaas, N. C., Chan, M. N., Loza, C. L., Kwan, A. J., Hersey, S. P., Flagan, R. C., Wennberg, P. O., and Seinfeld, J. H.: Reactive intermediates revealed in secondary organic aerosol formation from isoprene, *Proc. Natl. Acad. Sci. U. S. A.*, 107, 6640-6645, 10.1073/pnas.0911114107, 2010.
- Talbot, R. W., Andreae, M. O., Andreae, T. W., and Harriss, R. C.: Regional aerosol chemistry of the Amazon Basin during the dry season, *J. Geophys. Res.*, 93, 1499-1508, 1988.
- Talbot, R. W., Andreae, M. O., Berresheim, H., Artaxo, P., Garstang, M., Harriss, R. C., Beecher, K. M., and Li, S. M.: Aerosol chemistry during the wet season in central amazonia: The influence of long-range transport, *J. Geophys. Res.*, 95, 16955-16969, 1990.
- Trebs, I., Metzger, S., Meixner, F. X., Helas, G. N., Hoffer, A., Rudich, Y., Falkovich, A. H., Moura, M. A. L., da Silva, R. S., Artaxo, P., Slanina, J., and Andreae, M. O.: The  $\text{NH}_4^+$ - $\text{NO}_3^-$ - $\text{Cl}^-$ - $\text{SO}_4^{2-}$ - $\text{H}_2\text{O}$  aerosol system and its gas phase precursors at a pasture site in the Amazon Basin: How relevant are mineral cations and soluble organic acids?, *J. Geophys. Res.*, 110, D07303, 10.1029/2004JD005478, 2005.
- Ulbrich, I. M., Canagaratna, M. R., Zhang, Q., Worsnop, D. R., and Jimenez, J. L.: Interpretation of organic components from Positive Matrix Factorization of aerosol mass spectrometric data, *Atmos. Chem. Phys.*, 9, 2891-2918, 2009.
- Vaden, T. D., Imre, D., Beranek, J., Shrivastava, M., and Zelenyuk, A.: Evaporation kinetics and phase of laboratory and ambient secondary organic aerosol, *Proc. Natl. Acad. Sci. U. S. A.*, 108, 2190-2195, 10.1073/pnas.1013391108, 2011.
- Zhang, Q., Alfarra, M. R., Worsnop, D. R., Allan, J. D., Coe, H., Canagaratna, M. R., and Jimenez, J. L.: Deconvolution and quantification of hydrocarbon-like and oxygenated organic aerosols based on aerosol mass spectrometry, *Environ. Sci. Technol.*, 39, 4938-4952, 10.1021/es0485681, 2005.

Zhang, Q., Jimenez, J. L., Canagaratna, M. R., Ulbrich, I. M., Ng, N. L., Worsnop, D. R., and Sun, Y. L.: Understanding atmospheric organic aerosols via factor analysis of aerosol mass spectrometry: a review, *Anal. Bioanal. Chem.*, 401, 3045-3067, 10.1007/s00216-011-5355-y, 2011.

## List of Figures

**Figure 11.** Time series of observations during AMAZE-08. (a, b, c) Organic, sulfate, ammonium, nitrate, and chloride mass concentrations measured by AMS. (d) Black-carbon-equivalent mass concentrations measured by filter-based reflectance (fine-mode) analysis as well as optically derived by MAAP (637 nm) and aethalometer (660 nm) measurements. (e) Component mass fractions of panels a to d. For panel d, MAAP data were used. The inset pie chart represents the campaign average. (f) Scattering coefficient measured by nephelometry at 550 nm. Only particles of 7  $\mu\text{m}$  and smaller passed through the sampling inlet. (g) Elemental ratios O:C, H:C, N:C, and S:C for the submicron organic particles, as determined by high-resolution AMS data. Except for panel f, the data represent the submicron or fine-mode fraction of the ambient particle population. Concentrations are normalized to STP conditions (see main text). Periods in gray were influenced by local generator exhaust plume during times of local wind reversal and were excluded from the shown data sets and analysis.

**Figure 22.** Scatter plot of ammonium and sulfate mass concentrations (gray circles). The red symbols show campaign-average values reported in the literature for other measurements in the Amazon basin, both in the wet and dry seasons.

**Figure 33.** Diel profiles of (top) the temperature and relative humidity at the top of the measurement tower, (middle) normalized AMS-measured speciated mass concentrations (maximum concentrations in  $\mu\text{g m}^{-3}$  (STP) are shown in parentheses), and (bottom) percent occurrence of rain. Data represent mean values.

**Figure 44.** High-resolution mass spectra of secondary organic material produced in the Harvard Environmental Chamber by the oxidation of isoprene,  $\alpha$ -pinene, and  $\beta$ -

Formate  
or gramm

Formate  
or gramm

Formate  
or gramm

Formate  
or gramm

caryophyllene. The  $\text{NO}_x$  concentration was measured as  $< 1$  ppbv during these experiments and was estimated later as  $< 70$  ppt for typical operating of the HEC (Liu et al., 2013). The relative intensities of ions having  $m/z \geq 65$  were multiplied by 10. The intensities at each  $m/z$  represent three experiments that were performed at different SOM particle mass concentrations. A single intensity bar is color-coded by the contribution of different ion families (i.e., fragments containing C, H, O, or N for subscripts of  $x, y, z, i \geq 1$ ) as determined from analysis of the high-resolution spectra (Shilling et al., 2009). The relative intensities of the  $\text{H}_y\text{O}_1^+$  family were derived from the intensity of  $\text{CO}_2^+$  based on calibrations described in Chen et al. (2011).

**Figure 55.** Statistical factors HOA, OOA-1, OOA-2, and OOA-3 identified by PMF analysis.

The relative intensities of ions having  $m/z \geq 65$  were multiplied by 10.

**Figure 66.** Time series of the loadings for the factors HOA, OOA-1, OOA-2, and OOA-3 (left axes; dots) and time series of the concentrations of tracer species, including  $\text{NO}_x$ , CO, AMS chloride, AMS potassium, aethalometer black-carbon, MVK + MACR, isoprene, monoterpenes, and sesquiterpenes (right axes; lines). The BVOCs were measured by PTR-MS (Karl et al., 2009).

**Figure 77.** Comparison of the OOA-3 factor to a synthetic mass spectrum obtained from a linear combination of the mass spectra of laboratory-generated biogenic SOM (30%  $\alpha$ -pinene-derived SOM, 20%  $\beta$ -caryophyllene-derived SOM, and 50% isoprene-derived SOM at mass concentrations of 0.4 to 0.7  $\mu\text{g m}^{-3}$ ).

**Figure 88.** Campaign-average diel profiles of the loadings of the factors HOA, OOA-1, OOA-2, and OOA-3.

**Figure 99.** (top) Mass-diameter distributions measured by the AMS and the daytime wind rose

Formate  
or gramm

Formate  
or gramm

Formate  
or gramm

Formate  
or gramm

Formate  
or gramm

for the two time periods shown in the bottom panel. (upper bottom) Time series of daily mean temperature measured at the top of the measurement tower TT34. (lower bottom) Time series of the fractional contribution by each of the four statistical factors identified by PMF analysis (left axes) and the rain counts (right axes). Two case periods that differ significantly in the fractional contribution of PMF factors are selected.

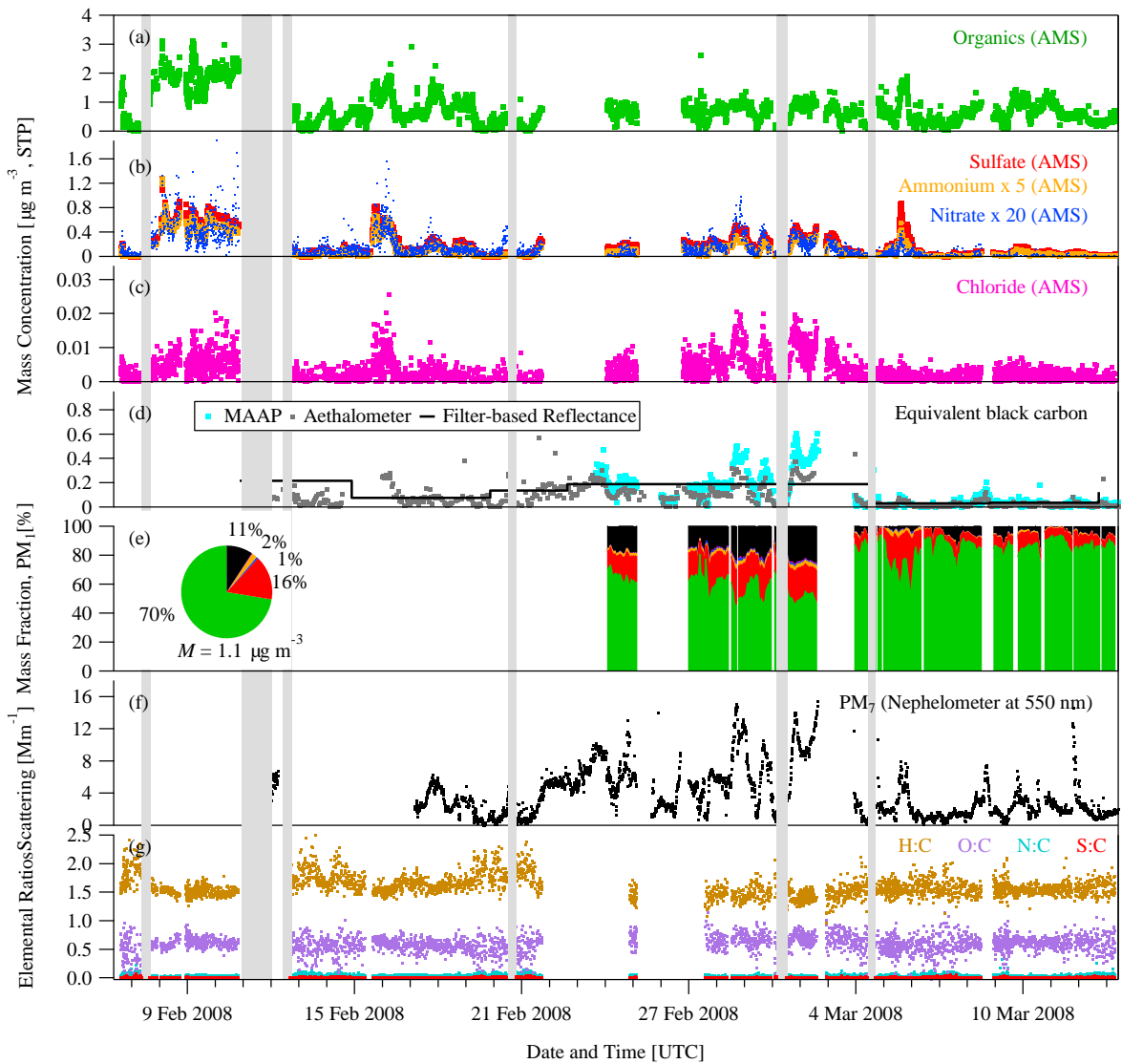


Figure 1



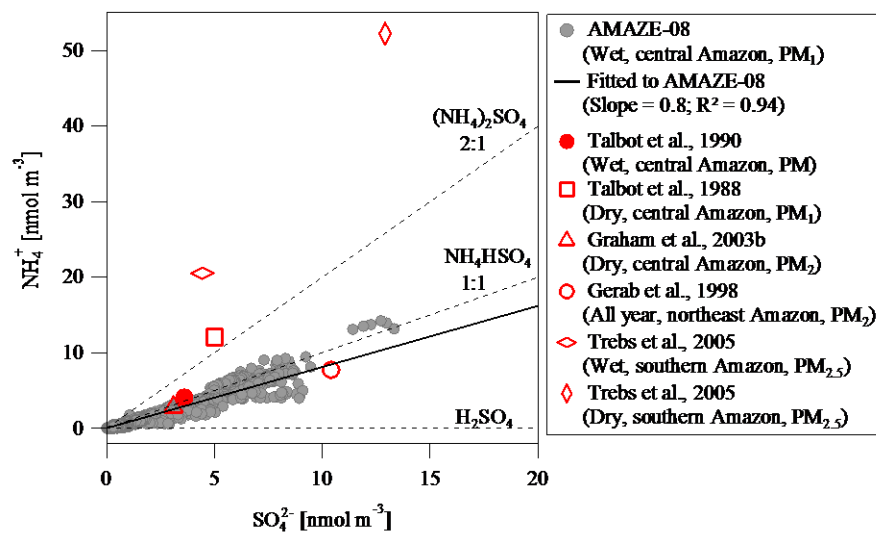


Figure 2

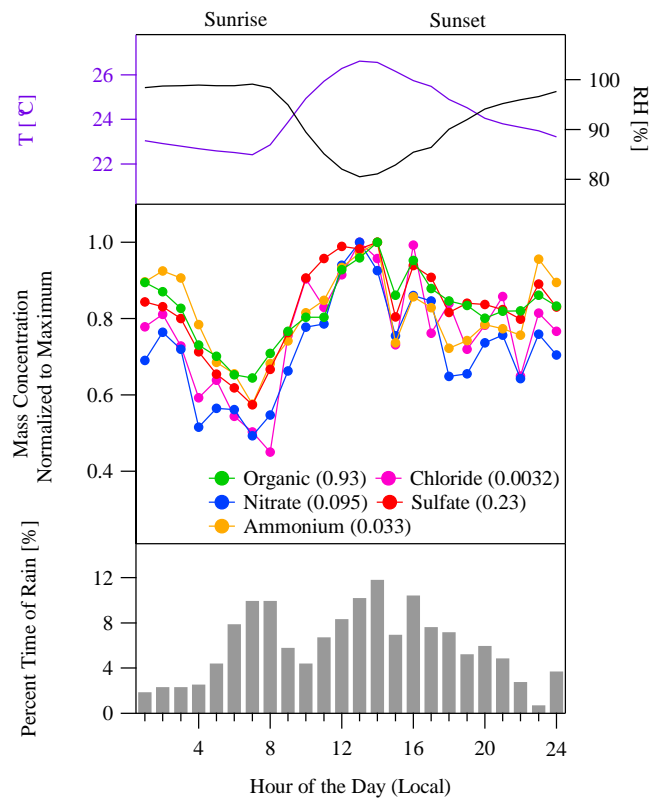


Figure 3

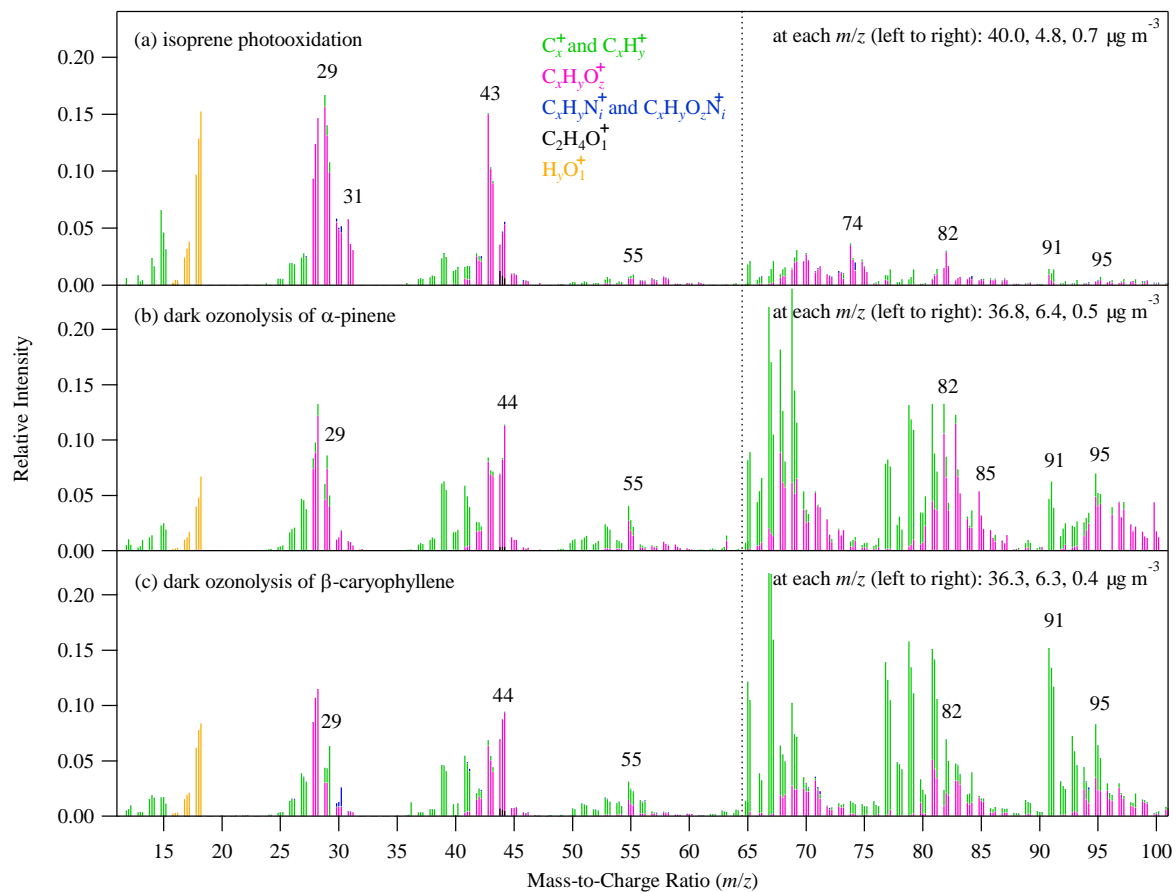


Figure 4

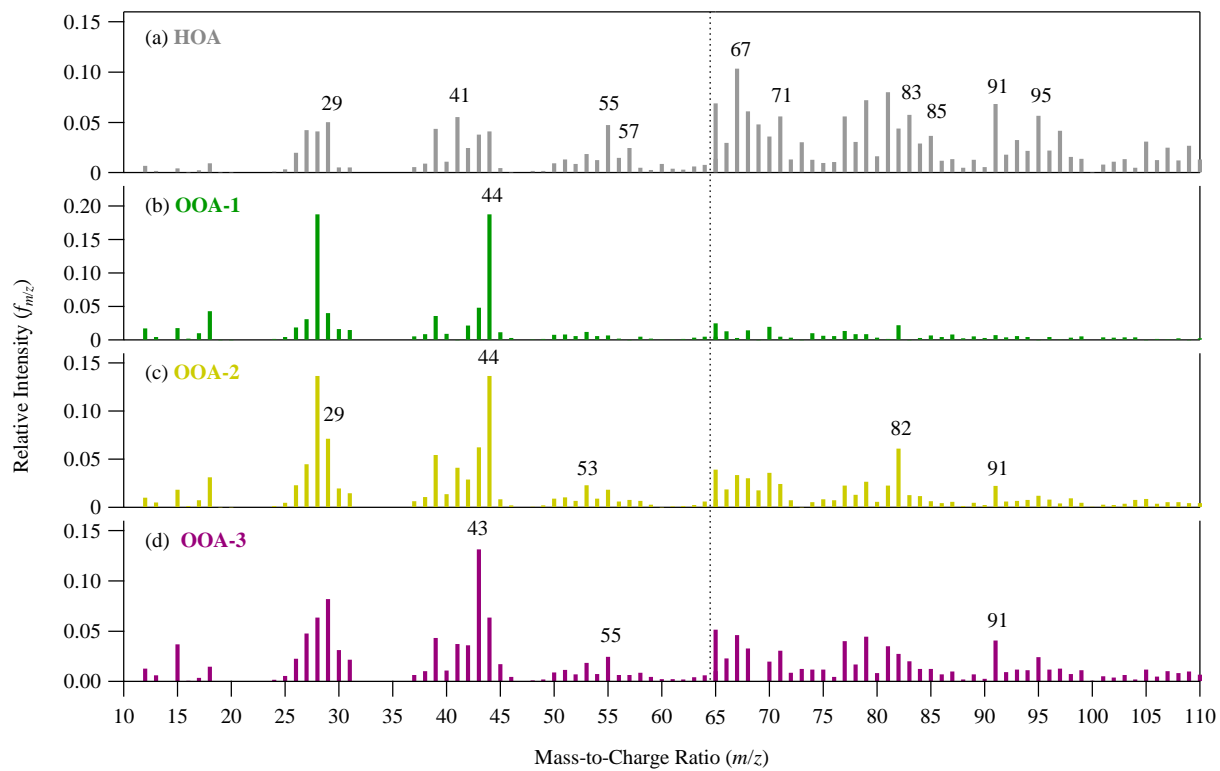


Figure 5

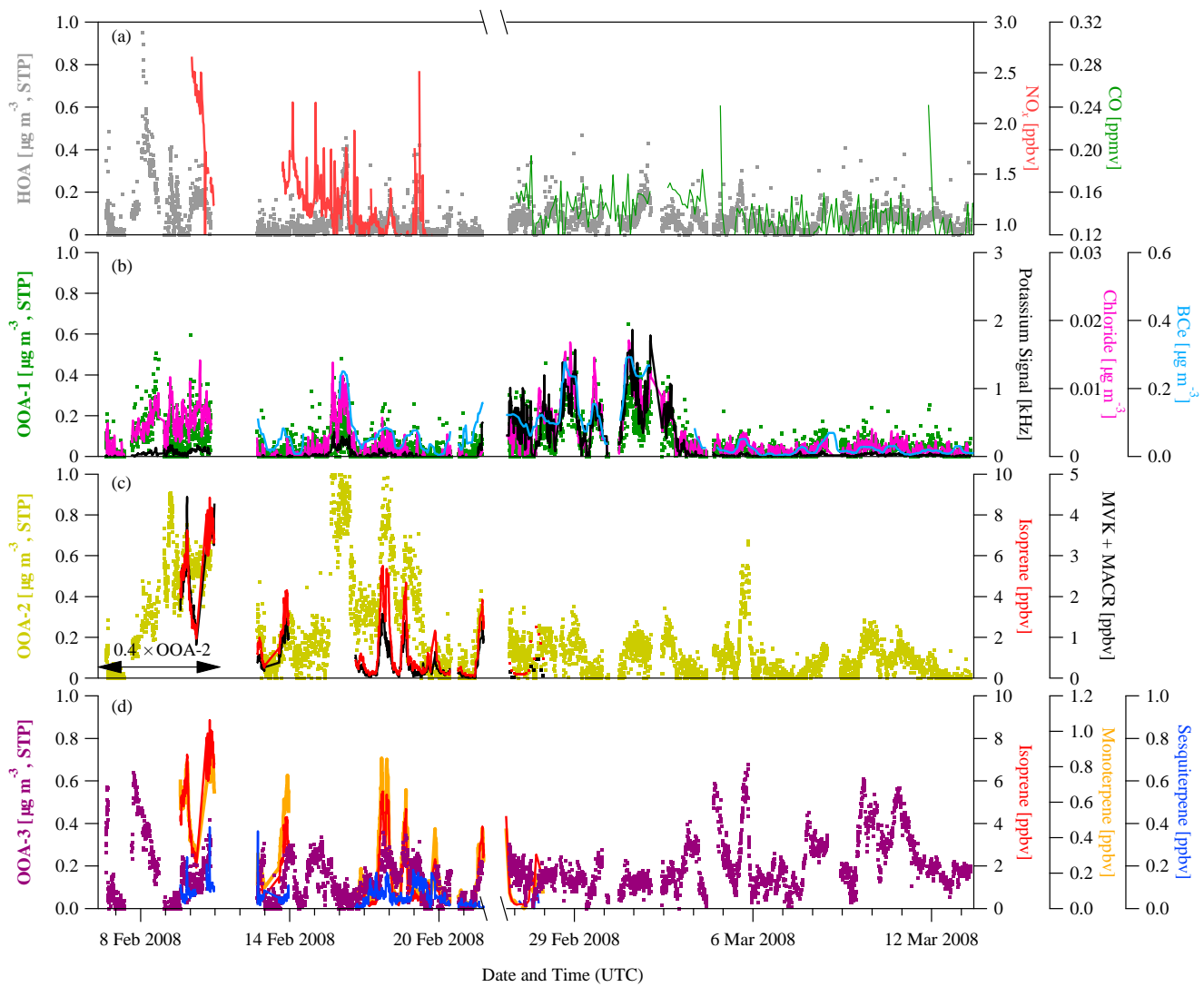


Figure 6

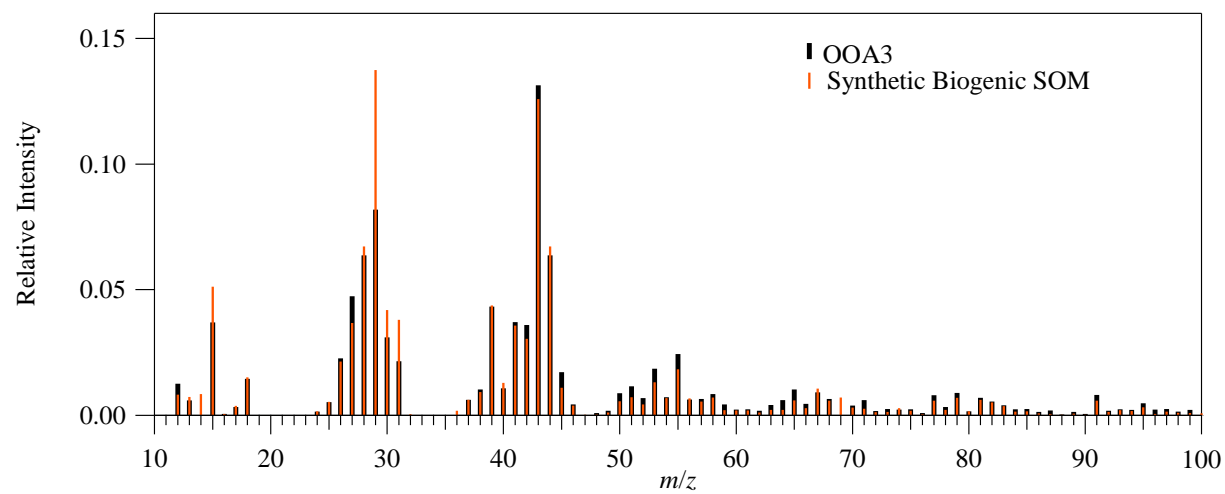


Figure 7

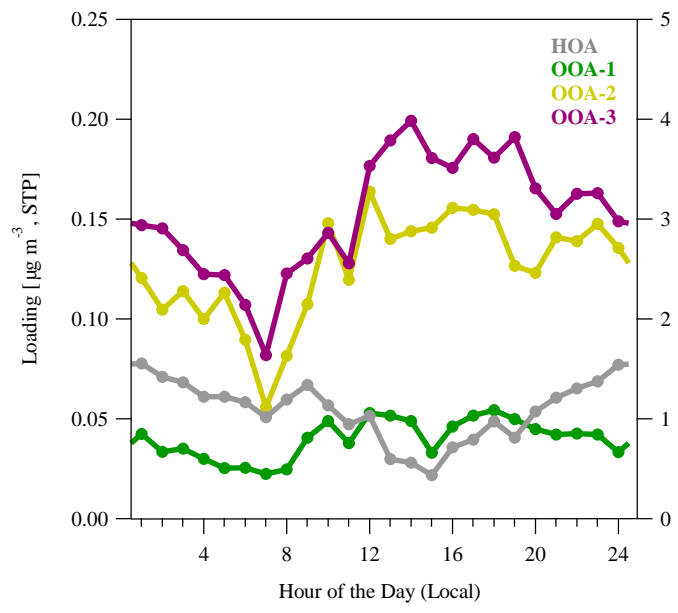


Figure 8

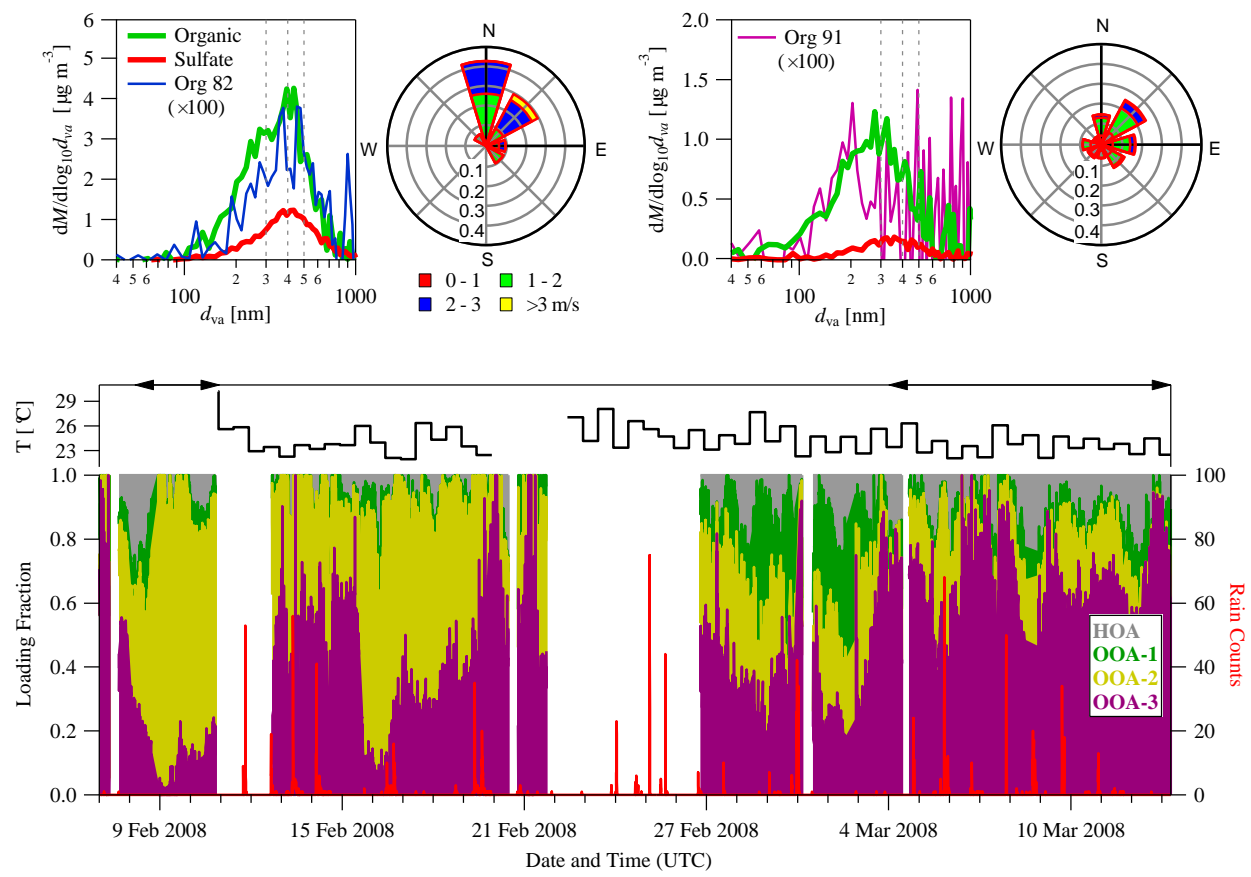


Figure 9



## Supplementary Material For Submicron Particle Mass Concentrations and Sources in the Amazonian Wet Season (AMAZE-08)

### A. AMS sampling and data processing

Chen et al. (2009) described the AMS sampling and data processing. Additional details are provided herein. Standard relative ionization efficiencies (RIE) were used in the analysis, including 1.1 for nitrate, 1.2 for sulfate, 1.4 for organic molecules, 4.0 for ammonium, 1.3 for chloride, and 2.0 for water (DeCarlo et al., 2006; Mensah et al., 2011). Unlike the analysis in Chen et al. (2009), the organic signals of  $C_3H^+$  at  $m/z$  37,  $C_3H_2^+$  at  $m/z$  38,  $C_3H_3^+$  at  $m/z$  39, and  $C_3H_4^+$  at  $m/z$  40, which made up 5-8% of the total organic signal, were calculated time-dependently based on the ratio of them to  $C_2H_2^+$  at  $m/z$  26. In the present study particle-phase water was not included in the calculations of species mass concentrations. Occasionally the sampling site was influenced by the exhaust plumes from the site power source, which was a diesel generator located 0.72 km from TT34 and typically downwind. Abrupt increases in AMS-measured sulfate mass concentrations, even greater than the organic concentrations, were indicators of influence by the local pollution source. These pollution events were defined herein and excluded from the data sets analyzed (Fig. 1). Chen et al. (2009) excluded more data by using a broader pollution filter defined by Martin et al. (2010).

The AMS detection limits, calculated as three times the standard deviation of mass concentrations for filtered air obtained at 150-s intervals, were 0.06, 0.02, 0.001, 0.006, 0.002  $\mu\text{g m}^{-3}$  for organic material, sulfate, ammonium, chloride, and nitrate, respectively. The AMS is capable of focusing particles with 30-1000 nm with size-dependent particle transmission efficiency (Liu et al., 2007). As described in Gunthe et al. (2009), we operated the AMS at

sampling pressures of 867–907 hPa. Under these conditions, the transmission efficiency is close to 100% for particles with vacuum aerodynamic diameter  $d_{va}$  of 100–400 nm and is greater than 20% for particles with  $d_{va}$  of 50–1000 nm. For organic measurements, the estimated uncertainty is 30% at concentrations of  $1 \mu\text{g m}^{-3}$  to 40% at concentrations of  $0.5 \mu\text{g m}^{-3}$ . It can increase to 100% for low organic concentrations ( $0.1 \mu\text{g m}^{-3}$ ). For sulfate measurements, the uncertainty is <10% for high concentrations ( $0.5 \mu\text{g m}^{-3}$ ) and about 40% for low concentrations ( $0.05 \mu\text{g m}^{-3}$ ).

Atomic ratios of oxygen-to-carbon (O:C), hydrogen-to-carbon (H:C), and nitrogen-to-carbon (N:C), as well as the mass ratios of organic material to organic carbon (OM:OC), were calculated from the W-mode data following previously described methods (Aiken et al., 2008). A recent study shows that organic aerosol with mixed keto-, hydroxyl-, and acid-functionalities readily undergoes thermally-induced dehydration and decarboxylation on the AMS vaporizer (Canagaratna et al., 2015). Such dehydration and decarboxylation can lead to much greater  $(\text{CO}^+)_{org}:(\text{CO}_2^+)_{org}$  and  $(\text{H}_2\text{O}^+)_{org}:(\text{CO}_2^+)_{org}$  ratios than the ones that have been empirically used in the “general” elemental analysis described by Aiken et al. (2008). A correction of 34% increase in O:C and 17% increase in H:C was applied based on the correction formula reported by Canagaratna et al. (2015).

In the AMS, the organosulfate species can fragment to organic ions ( $\text{C}_x\text{H}_y\text{O}_z^+$ ), organosulfur ions ( $\text{C}_x\text{H}_y\text{O}_z\text{S}^+$ ), and ions with a pattern indistinguishable from inorganic sulfate (e.g.,  $\text{SO}_2^+$ ) (Farmer et al., 2010). Similarly, the organonitrate species also fragment to the  $\text{NO}_x^+$  ions and are detected as inorganic nitrate by the AMS. For the AMAZE-08 data set, signal intensities for  $\text{C}_x\text{H}_y\text{O}_z\text{S}^+$  ions were not above noise in the collected high-resolution mass spectra. The agreement among AMS, [ion chromatography \(IC\)](#), and [particle-induced X-ray emission \(PIXE\)](#) sulfate mass concentrations, as well as the absence of organosulfur ions in the

high-resolution mass spectra, suggest minimal mass concentration of organosulfate species, at least at concentrations above uncertainty levels. Nitrate had a campaign-average concentration of  $7 \pm 2 \text{ ng m}^{-3}$ . This value was greater than the average fine-mode concentration of  $4 \pm 1 \text{ ng m}^{-3}$  measured by IC. As a test against possible significance of organonitrate species to the results of the present study, a limiting assumption that assigns all AMS-measured nitrate to organonitrate increases the average O:C ratio by  $<0.01$  for the elemental analysis and corresponds to a maximum of 5% contribution of organonitrates to the total organic particle mass concentration for an assumed molecular weight of  $360 \text{ g mol}^{-1}$  (Chen et al., 2011). The low mass concentration of particle-phase organonitrates is expected because of the low prevailing  $\text{NO}_x$  concentrations and humid environment (Day et al., 2010; Liu et al., 2012).

#### **B. Other concurrent measurements and comparisons among measurements**

Instruments making measurements during AMAZE-08 at the TT34 site are listed in Martin et al. (2010). The size distribution of particles between 0.010 and 0.48  $\mu\text{m}$  (mobility diameter) was measured every 5 min by a Scanning Mobility Particle Sizer (Lund SMPS) (Roldin [et al.](#), 2008). Particle volume concentrations were calculated from the SMPS size distributions for an assumption of spherical particles. The total number concentration for particles greater than 0.010  $\mu\text{m}$  was measured every 3 s by a Condensation Particle Counter (CPC, TSI 3010). Particle scattering coefficients at multiple wavelengths were measured every 1 min by a nephelometer (TSI 3563) and averaged to 10 min. The light absorption at 637 nm of deposited particles was measured every 1 min by the Multiangle Absorption Photometer (MAAP, Thermo 5012). These several instruments sampled through a laminar-flow line (i.e., separate sampling from the AMS line) that was characterized by lower and upper limits of transmission for particle diameters of 0.004 and 7  $\mu\text{m}$ , respectively (Martin et al., 2010). Several particle filter

samples were collected (Artaxo et al., 2013). Total-particle filters (TPF;  $PM_3$ ) were collected in-line with the turbulent inlet used by the AMS. Stacked filter units (SFU) were installed separately at 10 m to sample fine- ( $PM_2$ ) and coarse-mode particles ( $PM_{2-10}$ ). The two types of filters show reasonable agreement on the particle mass concentration (Table S2). The fine-mode data from the SFU are reported herein. Filter samples were analyzed by ~~ion chromatography~~ ~~(IC)~~IC for water-soluble ionic components, including sulfate, nitrate, and ammonium, among other components. The filters were also analyzed by ~~PIXE~~particle-induced X-ray emission ~~(PIXE)~~ for elemental composition. Concentrations were adjusted to STP conditions.

The AMS data can be compared to other concurrent measurements of AMAZE-08. The mass ratio of NR- $PM_1$  measured by the AMS to  $PM_2$  by filter assays was 0.65 as a campaign average (Table S2). The ratio was less than unity because  $PM_2$  included contributions by black carbon and mineral dust (Sect. 3.1) as well as organic material in the diameter range of 1 to 2  $\mu m$  (Pöschl et al., 2010). Particle mass-diameter distributions obtained from gravimetric analysis of stages of a Multi-Orifice Uniform Deposit Impactor (MOUDI) showed that an average of 30% of the particle mass concentration was associated with diameter range from 1 to 2  $\mu m$  (cf. Fig. 16 in Martin et al. (2010)).

Figure S6a shows a line of slope  $m$  of 1.24 and correlation  $R^2$  of 0.81 in a scatter plot between the AMS-calculated and the SMPS-derived particle volume concentrations. Figure S6b shows the scatter plot of the number concentrations obtained by integrating the SMPS measurements and those directly measured by the CPC. The slope of 0.6 ( $R^2 = 0.90$ ) indicates that the CPC measured more particles than the corresponding SMPS-derived quantity. The SMPS bias to particle undercounting can explain  $m > 1$  in the scatter plot of Fig. S6a. The scatter plot between sulfate particle mass concentrations measured by the AMS and those measured by

IC analysis of the filters is fit by a line of  $m = 0.90$  and  $R^2 = 0.50$  (Fig. S6c).

The combined AMS and SMPS data sets were used to estimate the particle effective density  $\rho_{\text{eff}}$  ( $\text{kg m}^{-3}$ ) based on an in-common mode diameter (Katrib et al., 2005). For nonporous spherical particles, material density  $\rho$  has the same values as  $\rho_{\text{eff}}$ , and this condition was assumed to hold in the performed data analysis. The organic material density  $\rho_{\text{org}}$  was then derived by assuming volume additivity and by using  $\rho_{\text{inorg}}$  of  $1780 \text{ kg m}^{-3}$  as ammonium bisulfate for the inorganic components. The estimated campaign-average value of  $\rho_{\text{eff}}$  for submicron Amazonian particles is  $1390 \pm 150 \text{ kg m}^{-3}$ . Figure S7 shows one example of the mass-diameter distribution measured by the AMS compared to that derived from the SMPS measurements. Assuming that the chemical components either do not mix or alternatively have a numerically small excess volume of mixing, we can derive  $\rho_{\text{org}}$  of  $1270 \pm 110 \text{ kg m}^{-3}$  based on the campaign-average chemical composition and a density of  $1770 \text{ kg m}^{-3}$  for all inorganic components (Cross et al., 2007). The value of  $\rho_{\text{org}}$  is consistent with the density of  $1200\text{-}1500 \text{ kg m}^{-3}$  observed for laboratory-generated biogenic secondary organic material (Bahreini et al., 2005; Shilling et al., 2009; Chen et al., 2012).

Figure S6d shows the linear regression of the light scattering derived from the AMS ( $\text{PM}_{10}$ ) and the nephelometer measurements ( $\text{PM}_{7}$ ), all for 550-nm wavelength. In total, 74 time periods having nearly identical mass concentrations of sulfate were selected to obtain the averaged particle mass-diameter distributions measured by the AMS. For comparison, nephelometer data at 550 nm were averaged for the same time periods. The mass-diameter distributions were multiplied by diameter-dependent mass extinction efficiencies ( $\text{m}^2 \text{ g}^{-1}$ ) to estimate light scattering coefficients. The mass extinction efficiencies were calculated at 550 nm using Mie theory for a refractive index of  $1.42 - 0.006i$  (Guyon et al., 2003). An agreement was found

between calculated and measured aerosol scattering coefficients, particularly for periods free of influence of long-range advection of mineral dust. During the period of 22 February to 3 March 2008, the ratio of the AMS volume concentration to the nephelometer scattering is high (Fig. S8b). Elevated mass concentrations of mineral dust are observed by the lidar measurements (Baars et al., 2011) and the filter-based PIXE analysis (Prenni et al., 2009). Local wind and Hysplit back trajectories showed a Manaus plume on March 1, 2008. The elevated scattering is, therefore, plausibly a combination of African advection and Manaus plume influence although the coarse-mode contribution from mineral dust is the major driving force of the a weak correlation ( $R^2 = 0.21$ ) between the nephelometer and AMS dataset. In contrast, a strong correlation ( $m = 0.62$ ;  $R^2 = 0.82$ ) of the two data sets is shown for other periods, suggesting a dominant contribution of the non-refractory submicron volume to the total particle scattering. This non-refractory submicron volume is mainly organic material. The scattering coefficients related to the submicron organic material can go up to  $6 \text{ Mm}^{-1}$  at 550 nm.

### C. Positive-Matrix Factorization

Positive-matrix factorization (PMF) is a receptor-based model using a weighted least squares method to identify patterns in data. With caveats, it can be a useful tool to derive the source profiles of organic components from AMS data sets (Ulbrich et al., 2009). In this study, the PMF analysis was conducted on the V-mode organic UMR spectra ( $m/z$  12 to 220). The spectra were analyzed using the SQUIRREL toolkit. Prior to PMF analysis, the data set was pre-filtered to remove inorganic contributions, and the analysis was carried out only on the residual data set of the organic component. Fifteen  $m/z$  values were omitted because of the absence of organic ions. The time periods associated with random spikes, abrupt increase in sulfate mass concentrations, and little temporal variation caused by the instrument adjustments (Fig. 1) were

removed. The error values were calculated using the method described by Ulbrich et al. (2009). Fragments having a signal-to-noise ratio less than 2 and fragments set proportionally to  $m/z$  44 were downweighted by increasing their error estimates (Ulbrich et al., 2009).  $C_xF_y$  ions contributed significantly to the signals at  $m/z$  69, 119, 131, 169, 181, and 219, indicating the contamination of Fomblin lubricating oil, possibly from instrument pumps at the site (Cross et al., 2009). These signals appeared always as one statistical factor, with a spiky time series for the loading of that factor. These fragments were downgraded by increasing their error by 100 times. The PMF analysis was conducted with (1) different model error and (2) different seed number. The former was introduced to add modeling uncertainty to the instrumental uncertainty, reflecting the errors that may occur when the true factors do not have constant mass spectra. The latter represents the pseudo-random starting values. Unless otherwise noted, results are presented for both the model error and the seed number of zero. PMF produces a fit to the data, which is called a solution. The solution contains a set of factors and concentrations. For AMAZE-08, four statistical factors were identified and labeled as HOA, OOA-1, OOA-2, and OOA-3 (Fig. 4). The four factors HOA, OOA-1, OOA-2, and OOA-3 respectively accounted for 2%, 18%, 14%, and 66% of the variance in the data matrix, implying a residual variance of <1%.

#### *Number $p$ of factors*

Several mathematical metrics were used to set the number  $p$  of factors. The ratio  $Q:Q_{exp}$  of the sum of the squares of the uncertainty-weighted residuals to the expected values decreased by 16%, 8%, 3%, and 3% for  $p$  increasing from 2 to 5. Three or more factors therefore significantly account for the variance of data. The residual was 1% for  $p = 2$  or 3 and < 0.3% for  $p = 4$ . Structure in the residual was significantly reduced by increasing from  $p$  of 3 to 4 (Fig. S9). For these reasons, a choice of  $p = 4$  was made for the PMF analysis.

The choice of  $p = 4$  was also evaluated with respect to factor similarity and correlations of the time series of the factors. Increasing the  $p$  from 4 to 5 resulted in strongly correlation ( $R^2 = 0.96$ ) among the factors (Fig. S10). No sufficient information from the correlations with other tracers exists to anticipate this correlation; correlation among factors for  $p$  of 5 is believed to arise from a splitting of real factors.

#### *Rotational ambiguity of solutions (FPEAK).*

*FPEAK* is the rotational parameter. For simplicity,  $FPEAK = 0$  was used as the best representation of the PMF solution for this study. The PMF solution was evaluated for uniqueness under linear transformations (“rotations”) by varying the *FPEAK* parameter (Ulbrich et al., 2009). Solutions with *FPEAK* between -0.6 and 0.6 increase  $Q:Q_{\text{exp}}$  by 1%. Figure S11 shows the time series of factor concentrations over this *FPEAK* range. Changes in time series are relatively small compared to the changes in the features of the factors. The largest change is for the HOA factor. This factor accounts for a low fraction of the total signal and hence its features can change without causing a great increase in the residual. The rotational uncertainty causes no conflicts in the interpretation of the PMF factors.

#### *Uncertainty of the solutions.*

The results of running the PMF analysis for different pseudo-random starting values (i.e., seeds of 0 to 10) show negligible changes in the factors ( $R^2 > 0.999$ ;  $m > 0.995$ ) and the time series of the concentrations ( $R^2 > 0.999$ ;  $m > 0.95$ ). Testing a “model error” of 5% in the PMF analysis leads to changes in the factor profiles ( $R^2 > 0.80$ ;  $m > 0.90$ ) and in the time series of concentrations ( $R^2 > 0.95$ ;  $m > 0.75$ ) that are close to tolerance.

Quantitative assessment of the uncertainty of the factors is also made by 100 bootstrapping runs (Ulbrich et al., 2009). The results show that the uncertainties in the time



series of the concentrations are 15% for the OOA-2 and OOA-3 factors and 30% for the OOA-1 and HOA factors. The uncertainties in the factor spectra are <4% for OOA-2 and OOA-3 and <9% for OOA-1 and HOA. The mass spectrum of the HOA factor has the largest uncertainty (Fig. S12).

## Literature Cited

- Aiken, A. C., Decarlo, P. F., Kroll, J. H., Worsnop, D. R., Huffman, J. A., Docherty, K. S., Ulbrich, I. M., Mohr, C., Kimmel, J. R., Sueper, D., Sun, Y., Zhang, Q., Trimborn, A., Northway, M., Ziemann, P. J., Canagaratna, M. R., Onasch, T. B., Alfarra, M. R., Prevot, A. S. H., Dommen, J., Duplissy, J., Metzger, A., Baltensperger, U., and Jimenez, J. L.: O/C and OM/OC ratios of primary, secondary, and ambient organic aerosols with high-resolution time-of-flight aerosol mass spectrometry, *Environ. Sci. Technol.*, 42, 4478-4485, 10.1021/es703009q, 2008.
- Artaxo, P., Rizzo, L. V., Brito, J. F., Barbosa, H. M. J., A., A., Sena, E. T., Cirino, G. G., Bastos, W., Martin, S. T., and Andreae, M. O.: Atmospheric aerosols in Amazonia and land use change: from natural biogenic to biomass burning conditions, *Faraday Discuss.*, 165, 1-31, 10.1039/c3fd00052d, 2013.
- Baars, H., Ansmann, A., Althausen, D., Engelmann, R., Artaxo, P., Pauliquevis, T., and Souza, R.: Further evidence for significant smoke transport from Africa to Amazonia, *Geophys. Res. Lett.*, 38, L20802, 10.1029/2011GL049200, 2011.
- Bahreini, R., Keywood, M. D., Ng, N. L., Varutbangkul, V., Gao, S., Flagan, R. C., Seinfeld, J. H., Worsnop, D. R., and Jimenez, J. L.: Measurements of secondary organic aerosol from oxidation of cycloalkenes, terpenes, and m-xylene using an Aerodyne aerosol mass spectrometer, *Environ. Sci. Technol.*, 39, 5674-5688, 10.1021/es048061a, 2005.
- Canagaratna, M. R., Jimenez, J. L., Kroll, J. H., Chen, Q., Kessler, S. H., Massoli, P., Hildebrandt Ruiz, L., Fortner, E., Williams, L. R., Wilson, K. R., Surratt, J. D., Donahue, N. M., Jayne, J. T., and Worsnop, D. R.: Elemental ratio measurements of organic compounds using aerosol mass spectrometry: characterization, improved calibration, and implications, *Atmos. Chem. Phys.*, 15, 253-272, 10.5194/acp-15-253-2015, 2015.
- Chen, Q., Farmer, D. K., Schneider, J., Zorn, S. R., Heald, C. L., Karl, T. G., Guenther, A., Allan, J. D., Robinson, N., Coe, H., Kimmel, J. R., Pauliquevis, T., Borrmann, S., ~~Posehl~~Pöschl, U., Andreae, M. O., Artaxo, P., Jimenez, J. L., and Martin, S. T.: Mass spectral characterization of submicron biogenic organic particles in the Amazon Basin, *Geophys. Res. Lett.*, 36, L20806, 10.1029/2009g1039880, 2009.
- Chen, Q., Liu, Y., Donahue, N. M., Shilling, J. E., and Martin, S. T.: Particle-phase chemistry of secondary organic material: Modeled compared to measured O:C and H:C elemental ratios provide constraints, *Environ. Sci. Technol.*, 45, 4763-4770, 10.1021/es104398s, 2011.
- Chen, Q., Li, Y. L., McKinney, K. A., Kuwata, M., and Martin, S. T.: Particle mass yield from  $\beta$ -caryophyllene ozonolysis, *Atmos. Chem. Phys.*, 12, 3165-3179, 10.5194/acp-12-3165-2012, 2012.
- Cross, E. S., Slowik, J. G., Davidovits, P., Allan, J. D., Worsnop, D. R., Jayne, J. T., Lewis, D. K., Canagaratna, M., and Onasch, T. B.: Laboratory and ambient particle density determinations using light scattering in conjunction with aerosol mass spectrometry, *Aerosol Sci. Technol.*, 41, 343-359, 10.1080/02786820701199736, 2007.

Cross, E. S., Onasch, T. B., Canagaratna, M., Jayne, J. T., Kimmel, J., Yu, X. Y., Alexander, M. L., Worsnop, D. R., and Davidovits, P.: Single particle characterization using a light scattering module coupled to a time-of-flight aerosol mass spectrometer, *Atmos. Chem. Phys.*, 9, 7769-7793, 2009.

Day, D. A., Liu, S., Russell, L. M., and Ziemann, P. J.: Organonitrate group concentrations in submicron particles with high nitrate and organic fractions in coastal southern California, *Atmos. Environ.*, 44, 1970-1979, 10.1016/j.atmosenv.2010.02.045, 2010.

DeCarlo, P. F., Kimmel, J. R., Trimborn, A., Northway, M. J., Jayne, J. T., Aiken, A. C., Gonin, M., Fuhrer, K., Horvath, T., Docherty, K. S., Worsnop, D. R., and Jimenez, J. L.: Field-deployable, high-resolution, time-of-flight aerosol mass spectrometer, *Anal. Chem.*, 78, 8281-8289, 10.1021/ac061249n, 2006.

~~Docherty, K. S., Stone, E. A., Ulbrich, I. M., DeCarlo, P. F., Snyder, D. C., Schauer, J. J., Peltier, R. E., Weber, R. J., Murphy, S. M., Seinfeld, J. H., Grover, B. D., Eatough, D. J., and Jimenez, J. L.: Apportionment of primary and secondary organic aerosols in southern California during the 2005 Study of Organic Aerosols in Riverside (SOAR-1), *Environ. Sci. Technol.*, 42, 7655-7662, 10.1021/es8008166, 2008.~~

Farmer, D. K., Matsunaga, A., Docherty, K. S., Surratt, J. D., Seinfeld, J. H., Ziemann, P. J., and Jimenez, J. L.: Response of an aerosol mass spectrometer to organonitrates and organosulfates and implications for atmospheric chemistry, *Proc. Natl. Acad. Sci. U. S. A.*, 107, 6670-6675, 10.1073/pnas.0912340107, 2010.

~~Gomez Gonzalez, Y., Surratt, J. D., Cuyekens, F., Szmigielski, R., Vermeylen, R., Jaoui, M., Lewandowski, M., Offenberg, J. H., Kleindienst, T. E., Edney, E. O., Blockhuys, F., Van Alsenoy, C., Maenhaut, W., and Claeys, M.: Characterization of organosulfates from the photooxidation of isoprene and unsaturated fatty acids in ambient aerosol using liquid chromatography/(-) electrospray ionization mass spectrometry, *J. Mass Spectrom.*, 43, 371-382, 10.1002/jms.1329, 2008.~~

Gunthe, S. S., King, S. M., Rose, D., Chen, Q., Roldin, P., Farmer, D. K., Jimenez, J. L., Artaxo, P., Andreae, M. O., Martin, S. T., and Pöschl, U.: Cloud condensation nuclei in pristine tropical rainforest air of Amazonia: size-resolved measurements and modeling of atmospheric aerosol composition and CCN activity, *Atmos. Chem. Phys.*, 9, 7551-7575, 10.5194/acp-9-7551-2009, 2009.

Guyon, P., Boucher, O., Graham, B., Beck, J., Mayol-Bracero, O. L., Roberts, G. C., Maenhaut, W., Artaxo, P., and Andreae, M. O.: Refractive index of aerosol particles over the Amazon tropical forest during LBA-EUSTACH 1999, *J. Aerosol Sci.*, 34, 883-907, 10.1016/s0021-8502(03)00052-1, 2003.

~~Iinuma, Y., Boge, O., Kahnt, A., and Herrmann, H.: Laboratory chamber studies on the formation of organosulfates from reactive uptake of monoterpene oxides, *Phys. Chem. Chem. Phys.*, 11, 7985-7997, 10.1039/b904025k, 2009.~~

- Katrib, Y., Martin, S. T., Rudich, Y., Davidovits, P., Jayne, J. T., and Worsnop, D. R.: Density changes of aerosol particles as a result of chemical reaction, *Atmos. Chem. Phys.*, 5, 275-291, 2005.
- Liu, P. S. K., Deng, R., Smith, K. A., Williams, L. R., Jayne, J. T., Canagaratna, M. R., Moore, K., Onasch, T. B., Worsnop, D. R., and Deshler, T.: Transmission efficiency of an aerodynamic focusing lens system: Comparison of model calculations and laboratory measurements for the Aerodyne Aerosol Mass Spectrometer, *Aerosol Sci. Technol.*, 41, 721-733, 10.1080/02786820701422278, 2007.
- Liu, S., Shilling, J. E., Song, C., Hiranuma, N., Zaveri, R. A., and Russell, L. M.: Hydrolysis of organonitrate functional groups in aerosol particles, *Aerosol Sci. Technol.*, 46, 1359-1369, 10.1080/02786826.2012.716175, 2012.
- Martin, S. T., Andreae, M. O., Althausen, D., Artaxo, P., Baars, H., Borrmann, S., Chen, Q., Farmer, D. K., Guenther, A., Gunthe, S. S., Jimenez, J. L., Karl, T., Longo, K., Manzi, A., Muller, T., Pauliquevis, T., Petters, M. D., Prenni, A. J., ~~Pöschl, U.~~, Rizzo, L. V., Schneider, J., Smith, J. N., Swietlicki, E., Tota, J., Wang, J., Wiedensohler, A., and Zorn, S. R.: An overview of the Amazonian Aerosol Characterization Experiment 2008 (AMAZE-08), *Atmos. Chem. Phys.*, 10, 11415-11438, 10.5194/acp-10-11415-2010, 2010.
- Mensah, A. A., Buchholz, A., Mentel, T. F., Tillmann, R., and Kiendler-Scharr, A.: Aerosol mass spectrometric measurements of stable crystal hydrates of oxalates and inferred relative ionization efficiency of water, *J. Aerosol Sci.*, 42, 11-19, 10.1016/j.jaerosci.2010.10.003, 2011.
- Pöschl, U., Martin, S. T., Sinha, B., Chen, Q., Gunthe, S. S., Huffman, J. A., Borrmann, S., Farmer, D. K., Garland, R. M., Helas, G., Jimenez, J. L., King, S. M., Manzi, A., Mikhailov, E., Pauliquevis, T., Petters, M. D., Prenni, A. J., Roldin, P., Rose, D., Schneider, J., Su, H., Zorn, S. R., Artaxo, P., and Andreae, M. O.: Rainforest aerosols as biogenic nuclei of clouds and precipitation in the Amazon, *Science*, 329, 1513-1516, 10.1126/science.1191056, 2010.
- Prenni, A. J., Petters, M. D., Kreidenweis, S. M., Heald, C. L., Martin, S. T., Artaxo, P., Garland, R. M., Wollny, A. G., and ~~Pöschl, U.~~: Relative roles of biogenic emissions and Saharan dust as ice nuclei in the Amazon basin, *Nature Geoscience*, 2, 401-404, Doi 10.1038/Ngeo517, 2009.
- Roldin, P., Nilsson, E., Swietlicki, E., Massling, A., and Zhou, J.: *Lund SMPS User's manual*, EUCAARI Brazil Version, 2008.
- Shilling, J. E., Chen, Q., King, S. M., Rosenoern, T., Kroll, J. H., Worsnop, D. R., DeCarlo, P. F., Aiken, A. C., Sueper, D., Jimenez, J. L., and Martin, S. T.: Loading-dependent elemental composition of  $\alpha$ -pinene SOA particles, *Atmos. Chem. Phys.*, 9, 771-782, 10.5194/acp-9-771-2009, 2009.
- ~~Surratt, J. D., Gomez-Gonzalez, Y., Chan, A. W. H., Vermeylen, R., Shahgholi, M., Kleindienst, T. E., Edney, E. O., Offenberg, J. H., Lewandowski, M., Jaoui, M., Maenhaut, W., Claeys, M., Flagan, R. C., and Seinfeld, J. H.: Organosulfate formation in biogenic secondary organic aerosol, *J. Phys. Chem. A*, 112, 8345-8378, 10.1021/jp802310p, 2008.~~

Ulbrich, I. M., Canagaratna, M. R., Zhang, Q., Worsnop, D. R., and Jimenez, J. L.: Interpretation of organic components from Positive Matrix Factorization of aerosol mass spectrometric data, *Atmos. Chem. Phys.*, 9, 2891-2918, 2009.

**Table S11.** Summary of the regression coefficients  $m$  of instrument comparisons. Expected  $m$  values are shown in parentheses. These values are estimated on the basis of the diameter domain of the various instruments and an assumed AMS collection efficiency of 1.0, in conjunction with typical mass size distributions obtained by MOUDI measurements during the wet season in the Amazon basin (Martin et al., 2010; Pöschl et al., 2010).

**Formatted:** Font: Times New Roman, 12 pt, Bold, Do not check spelling or grammar

	Volume concentration	Number concentration	Sulfate mass concentration	Particle mass concentration	Light scattering at 550 nm
	SMPS	CPC	Filter-based	Filter-based	Nephelometer
AMS	1.24 (1.0)	-	0.90 (1.0)	0.65 (0.7)	0.62 (< 1.0)
SMPS	-	0.59 (< 1.0)	-	-	

**Table S22.** Summary of the particle mass concentration ( $\mu\text{g m}^{-3}$ , STP) measured by the stacked filter units on the 10-m inlet (SFU), by the total-particle filter on the 38-m turbulent inlet (TPF), and by the AMS during AMAZE-08.

**Formatted:** Font: Times New Roman, 12 pt, Bold, Do not check spelling or grammar

Sampling Periods (MM/DD/YY)	SFU: PM <sub>2</sub>	TPF: PM <sub>3</sub>	AMS: NR-PM <sub>1</sub>	AMS/SFU	AMS/TPF
02/10/08 – 02/14/08	2.51	n.a.	1.75	0.70	n.a.
02/14/08 – 02/16/08	1.41		1.37	0.97	
02/16/08 – 02/19/08	0.87	1.30	0.89	1.02	0.87
02/19/08 – 02/22/08	1.14	1.48	0.85	0.75	0.57
02/22/08 – 02/26/08	2.44		0.85	0.35	
02/26/08 – 02/29/08	3.20	2.86	0.96	0.30	0.33
02/29/08 – 03/04/08	3.38		0.99	0.29	
03/04/08 – 03/08/08	1.02	1.02	0.73	0.72	0.72
03/08/08 – 03/12/08	1.01	1.09	0.74	0.73	0.68
<b>Average</b>	<b>1.89</b>	<b>1.55</b>	<b>1.02</b>	<b>0.65</b>	<b>0.63</b>

## List of Figures

**Figure S11.** Map of the sampling site.

**Formatted:** Font: Times New Roman, 12 pt, Bold, Do not check spelling or grammar

**Figure S22.** Campaign-average pie chart of the composition of submicron particles, including the estimated contribution by mineral dust.

**Formatted:** Font: Times New Roman, 12 pt, Bold, Do not check spelling or grammar

**Figure S33.** Scatter plot of the mass concentrations (STP) of components derived from the AMS measurements.

**Formatted:** Font: Times New Roman, 12 pt, Bold, Do not check spelling or grammar

**Figure S44.** Example of the variations of component concentrations and O:C ratios before and after a rain event.

**Formatted:** Font: Times New Roman, 12 pt, Bold, Do not check spelling or grammar

**Figure S55.** Scatter plot of O:C versus  $I_{44}:I_{org}$  for biogenic secondary organic material produced in the Harvard Environmental Chamber. Also shown is the empirical relationship between O:C and  $I_{44}:I_{org}$  presented in Aiken et al. (2008) for Mexico City. Marker size corresponds to mass concentration for the laboratory measurements.

**Formatted:** Font: Times New Roman, 12 pt, Bold, Do not check spelling or grammar

**Figure S66.** Scatter plots among data sets. (a) AMS and SMPS volume concentrations for a particle material density calculated by using component densities of 1270, 1780, 1720, and 1520 kg m<sup>-3</sup> for organic material, ammonium bisulfate, ammonium nitrate, and ammonium chloride, respectively, and assuming volume additivity. The AMS data in this plot were averaged to the SMPS timebase. (b) SMPS and CPC total number concentrations. The CPC data were averaged to the SMPS timebase. (c) AMS and filter-based IC/PIXE sulfate mass concentrations. The AMS data were averaged to the periods of filter collection. The filter data include SFU PM<sub>2</sub> and TPF PM<sub>3</sub>. (d) AMS-derived and nephelometry-measured light scattering. For the AMS analysis, the measured size distributions were used as input to Mie calculations (see main text). The nephelometer data were averaged to the same

**Formatted:** Font: Bold, Do not check spelling or grammar

periods as the AMS mass-diameter distributions. Valued in all panels are normalized to STP.

**Figure S77.** Example of the mass-diameter distribution measured by the AMS compared to that derived from the SMPS measurements. The effective particle density  $\rho_{\text{eff}}$  is determined by the mode diameters. The SMPS mass-diameter distributions were derived by multiplying the SMPS volume-diameter distributions by  $\rho_{\text{eff}}$ . Data were sampled on March 11, 2008.

**Formatted:** Font: Times New Roman, 12 pt, Bold, Do not check spelling or grammar

**Figure S88.** (a) Time series of the particle volume concentrations obtained by the AMS and the SMPS measurements. (b) The ratio of the particle volume concentrations derived from the AMS measurements to the  $\text{PM}_{7.5}$  light scattering coefficients measured by the nephelometer at 550 nm. The AMS data were averaged to the nephelometer timebase. Gray areas represent the periods that were influenced by the generator exhaust plumes.

**Formatted:** Font: Times New Roman, 12 pt, Bold, Do not check spelling or grammar

**Figure S99.** Time series of the model residuals  $e_{ij}$  for the PMF analysis with *FPEAK* of zero. Terms include factor  $j$ , time  $i$ , and error  $\sigma$ .

**Formatted:** Font: Times New Roman, 12 pt, Bold, Do not check spelling or grammar

**Figure S1010.** Pearson's R (black dots) for the correlations between the time series and the mass spectra of any two factors (tagged as  $x\_y$ ) for the PMF solutions for a preset of different number of factors ( $p$ ).

**Formatted:** Font: Times New Roman, 12 pt, Bold, Do not check spelling or grammar

**Figure S1111.** (a) The mass spectra of the statistical factors identified by the PMF analysis for four-factor solutions and selected *FPEAK* ( $f_{\text{peak}}$ ) values. (b) Time series of mass concentrations for the statistical factors.

**Formatted:** Font: Times New Roman, 12 pt, Bold, Do not check spelling or grammar

**Figure S1212.** The mass spectrum of HOA from the bootstrapping analysis of four-factor PMF solutions. Average (black) with  $1-\sigma$  error bars (red) are shown.

**Formatted:** Font: Times New Roman, 12 pt, Bold, Do not check spelling or grammar



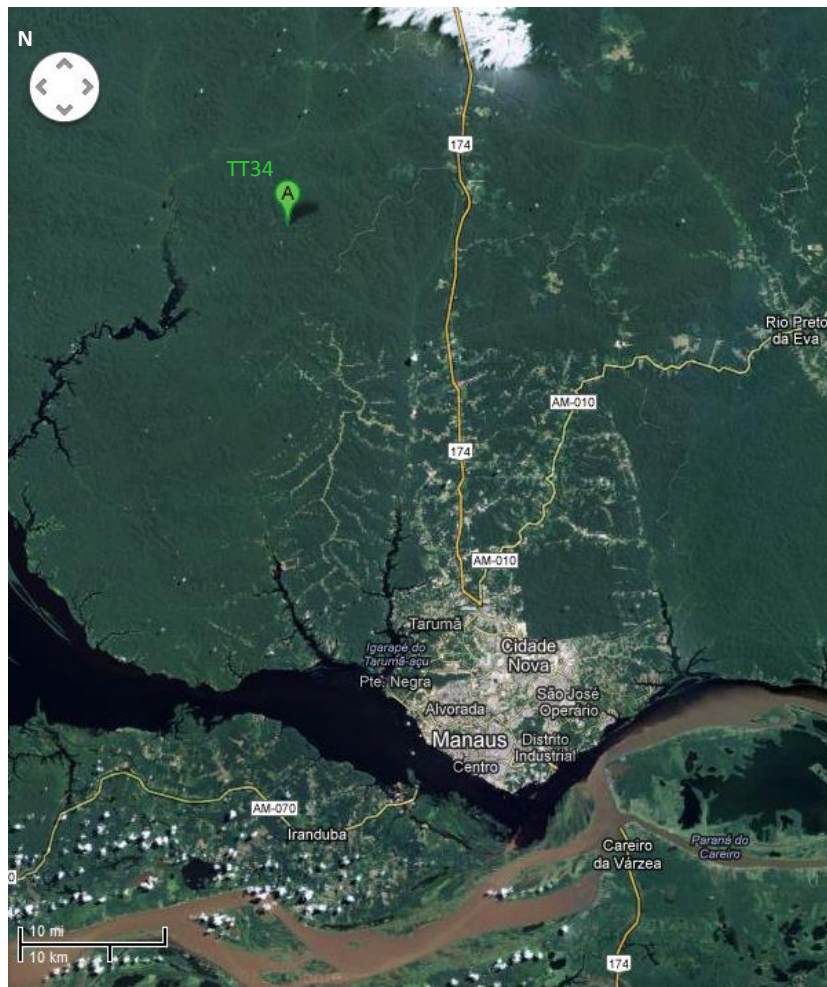


Figure S1

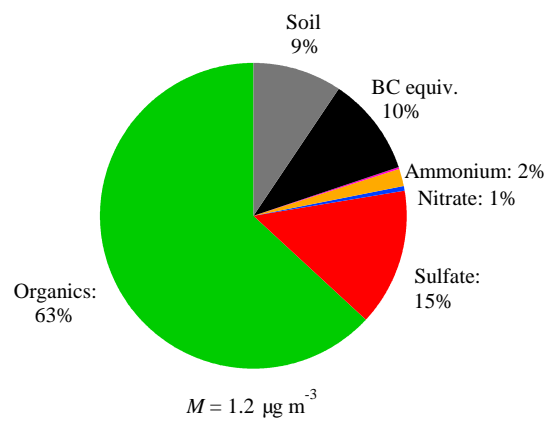


Figure S2

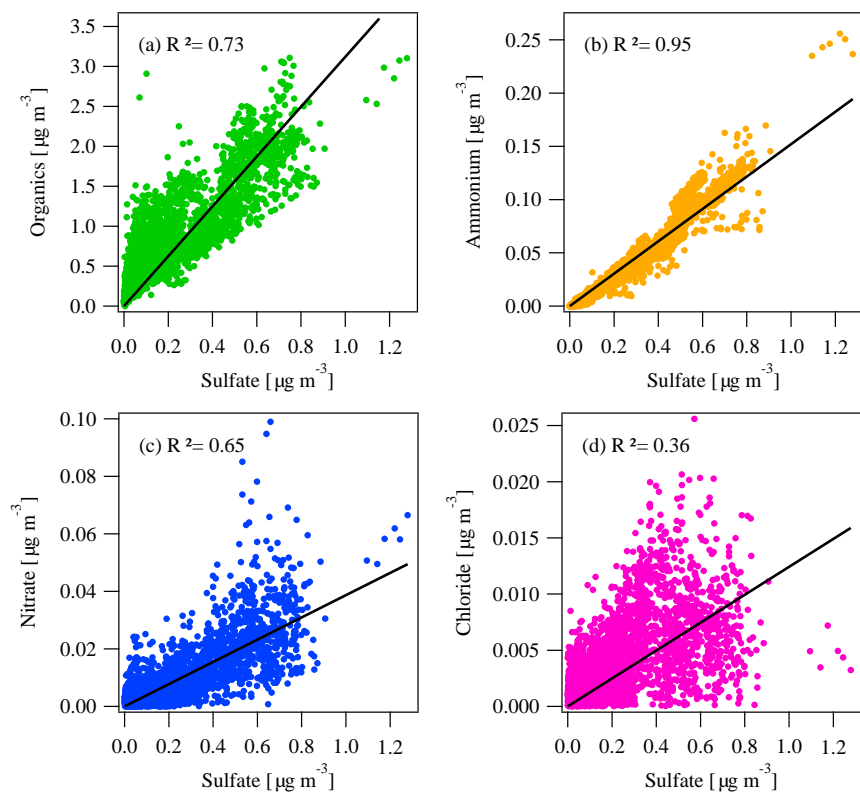


Figure S3

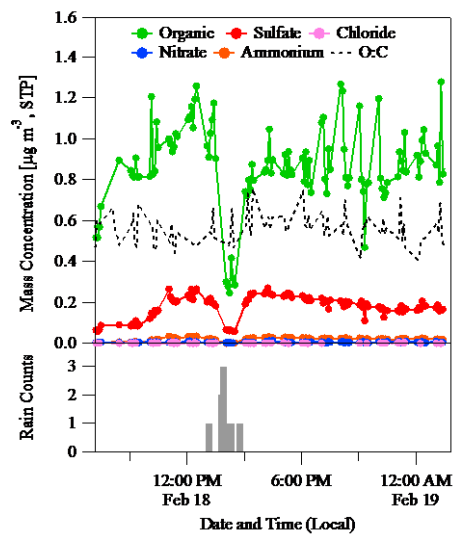


Figure S4

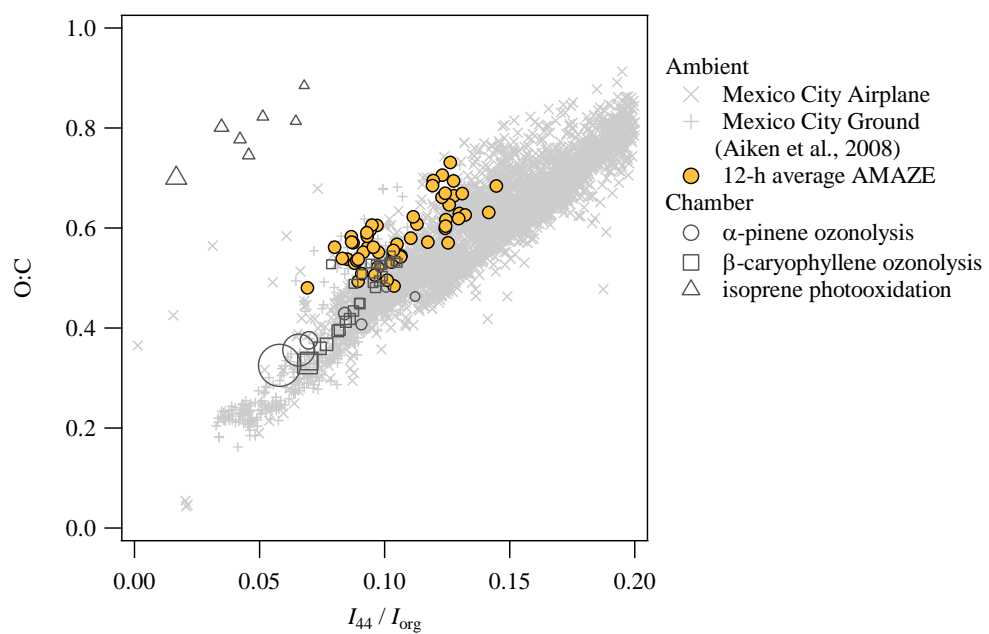


Figure S5

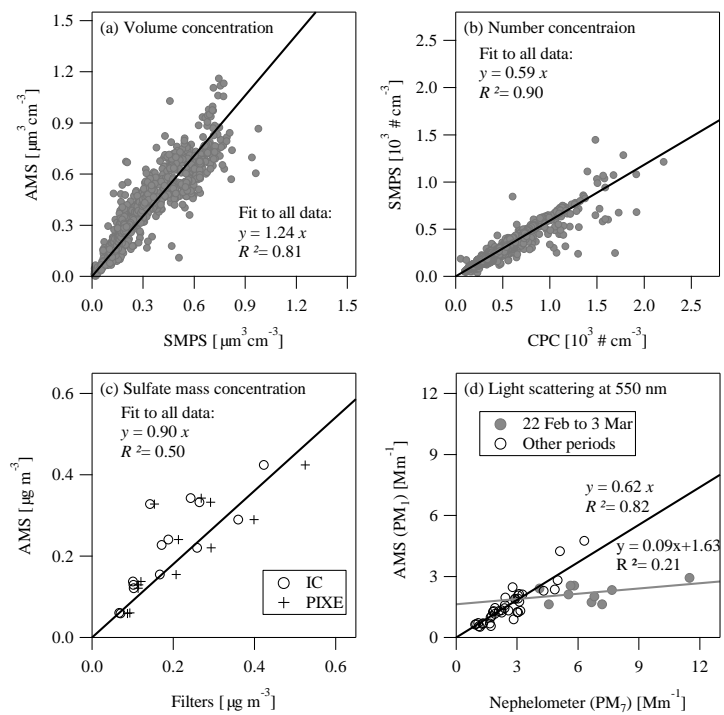


Figure S6

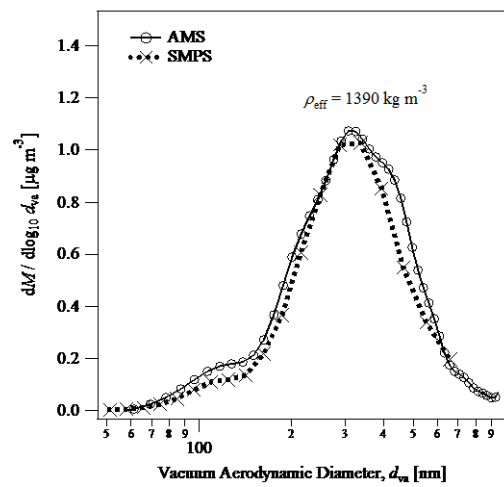


Figure S7

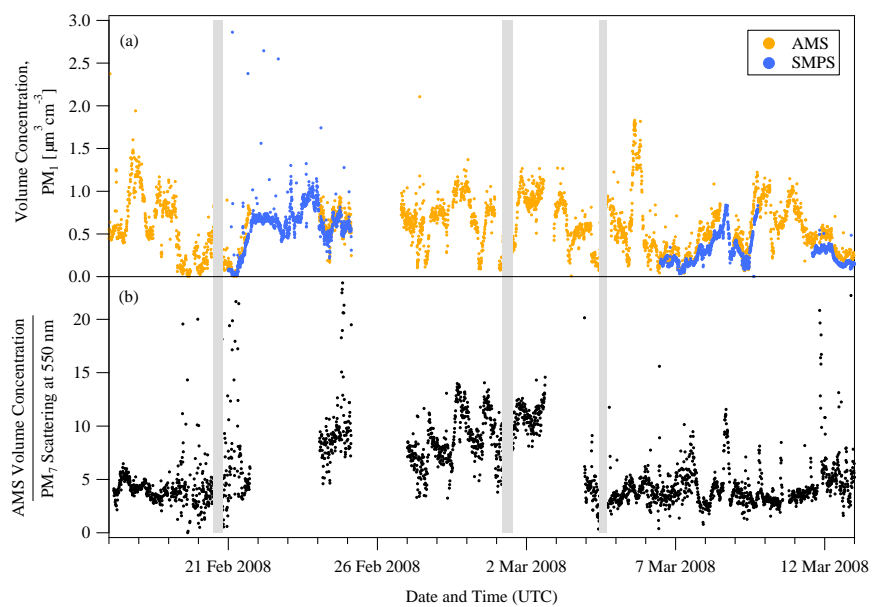


Figure S8



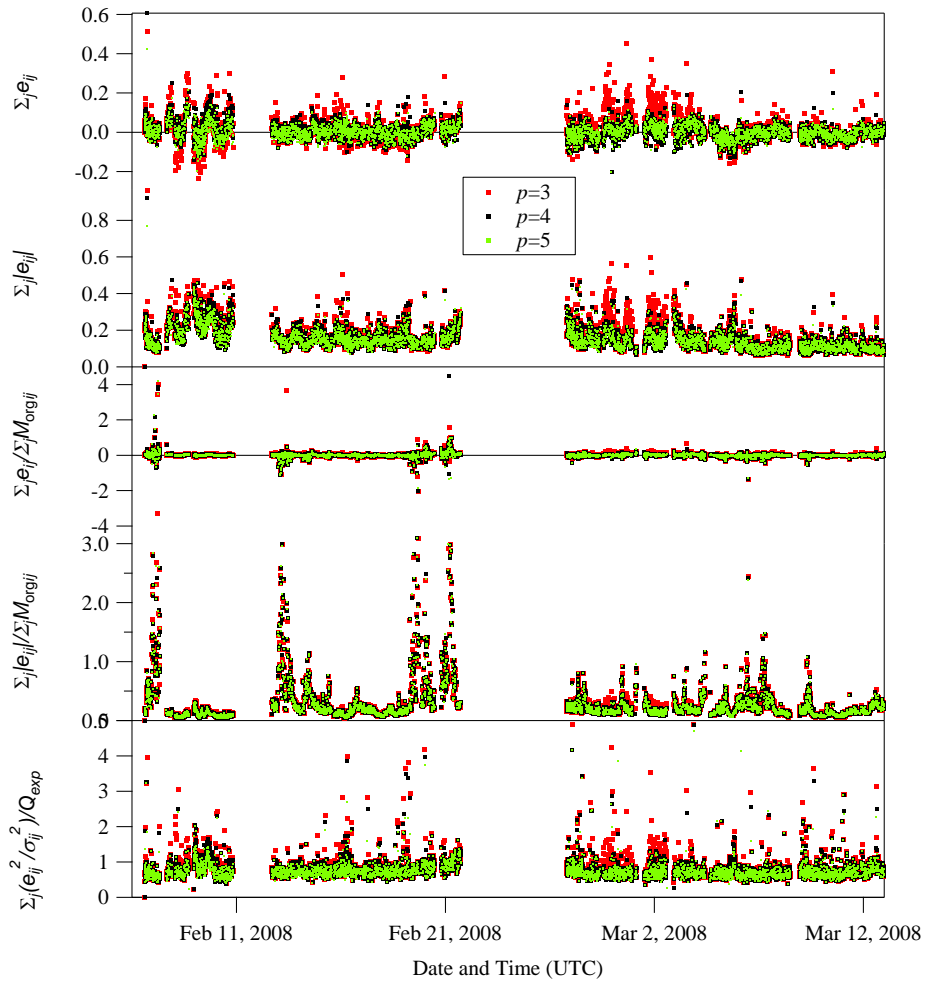


Figure S9

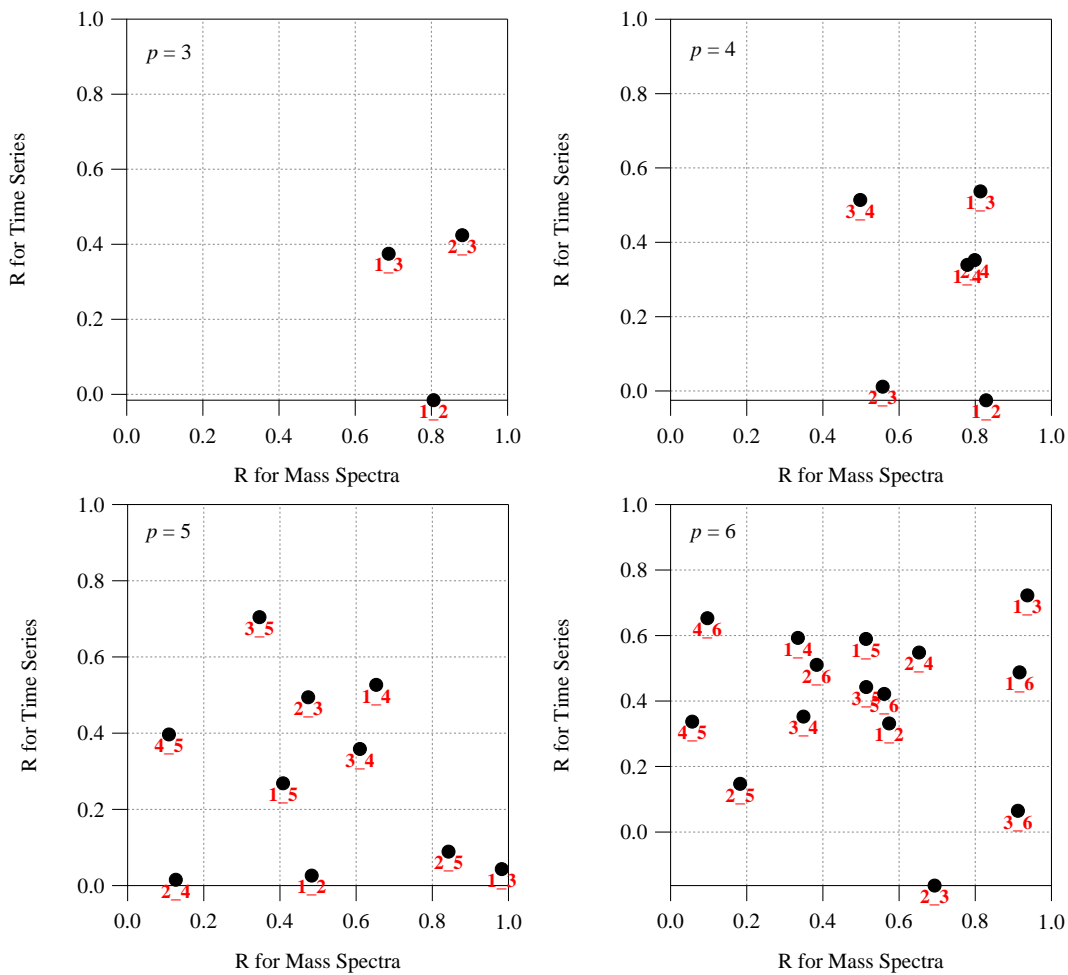


Figure S10

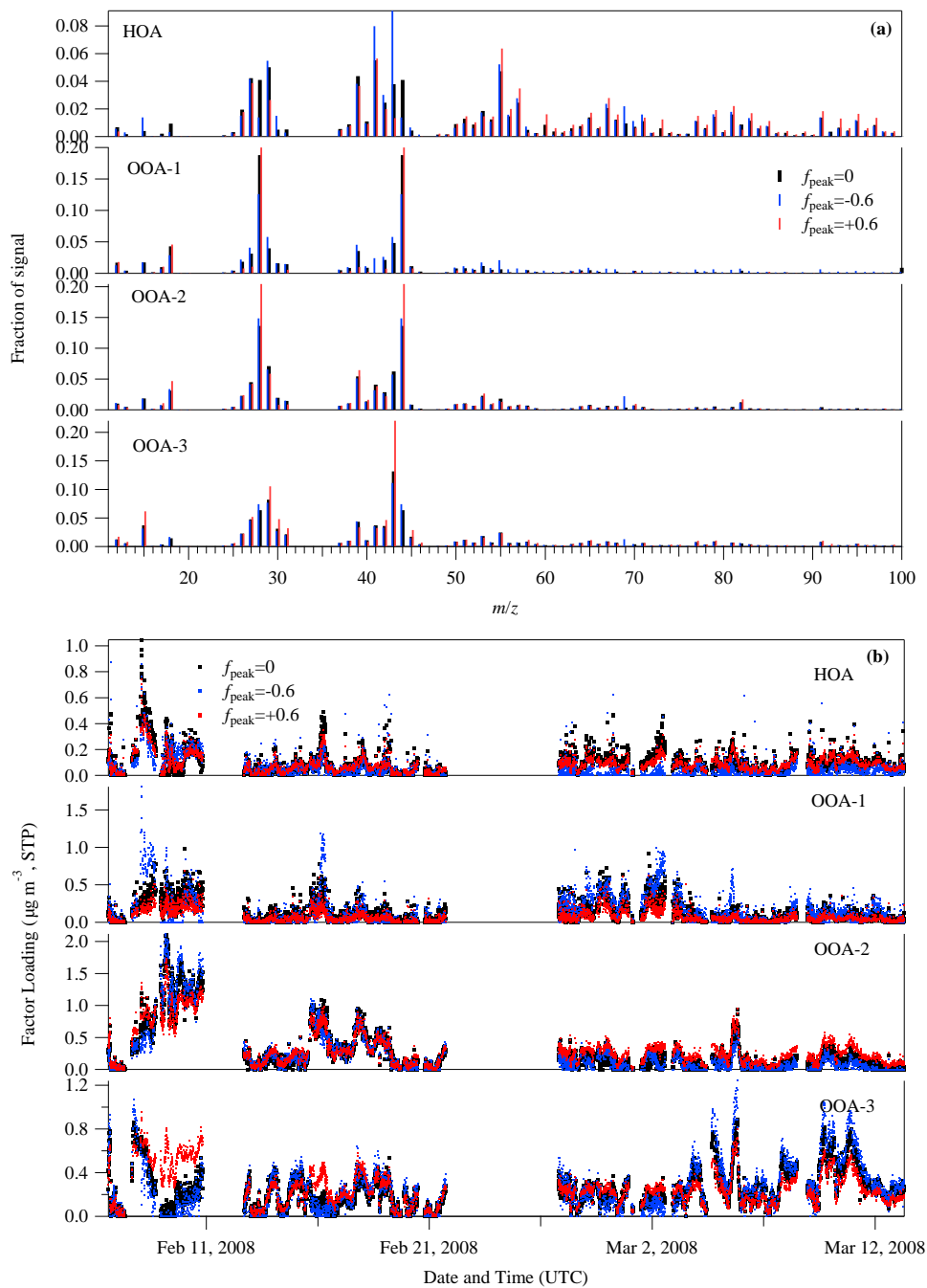


Figure S11

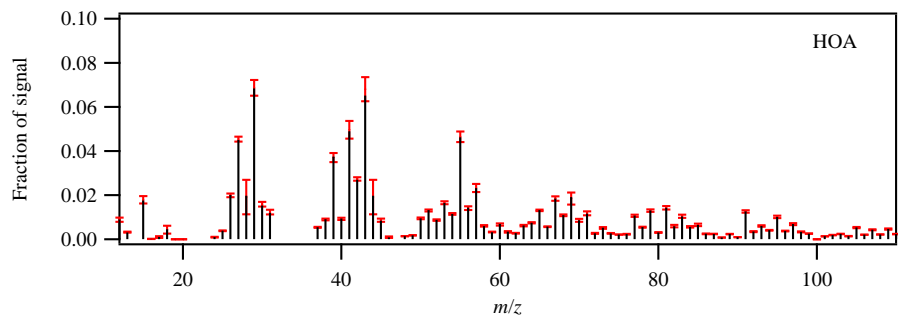


Figure S12